

Contents lists available at ScienceDirect

Petroleum Science

journal homepage: www.keaipublishing.com/en/journals/petroleum-science



Original Paper

A thermo-associating copolymer integrated with biogenic nanosilica as a novel viscosifier in low solid drilling fluids



Alain Pierre Tchameni a , Robert Dery Nagre b , Shu-Ming Yin a , Li-Qiang Wang a , Xiu-Ying Wang c , Si-Yuan Zhou d , Guan-Qun Hou d , Xu-Dong Wang a , **

- ^a College of Petroleum Engineering, Shandong Institute of Petroleum and Chemical Technology, Dongying, 257061, Shandong, China
- ^b Department of Oil and Gas Engineering, Kumasi Technical University, P.O. Box 854, Ghana
- ^c Shandong Provincial Institute of Physical and Chemical Exploration, Jinan, 250000, Shandong, China
- d CNPC GWDC Drilling Fluids Co., Ltd, Panjin, 124000, Liaoning, China

ARTICLE INFO

Article history: Received 23 August 2024 Received in revised form 21 April 2025 Accepted 21 April 2025 Available online 23 April 2025

Edited by Jia-Jia Fei

Keywords:
Polymer nano-hybrid
Thermo-associating copolymer
Biogenic nanosilica
Rheological properties
High temperature
Low-solid drilling fluids

ABSTRACT

Smart low-solid drilling fluids (SLSDFs) with thermo-controllable rheological properties and attractive thickening characteristics have recently captivated profound attention due to their low formation damage and enhanced cuttings lifting capacity. However, their applications to deep hole drilling at high temperatures have remained limited because of the thermal instability and environmental constraints of the thermo-associating polymers as additives. This work explored the synergistic benefits of thermoassociating polymer and biogenic nano-silica (B-SiNP) extracted from rice husk to improve the thermo-stability of SLSDF. This study shows that the nano-hybrid, TAP-S based on vinyl-terminated B-SiNP could potentially mitigate the limiting performance of conventional LSDF (F-2) caused by the failure of thermo-associating copolymers under elevated temperatures. TAP-S bearing drilling fluid (F-3) could preserve more than 5.6-fold of its initial properties (ca. apparent viscosity, plastic viscosity, yield point, and gel strength) with a nearly flat-gel profile in the temperature range of 25–230 °C, which was higher than those of the counterpart F-2 and base fluid according to the results of rheological tests analysis. In addition, TAP-S exhibited an abrupt thermo-thickening characteristic with a magnitude declining by only 1.05-fold and the activation Gibbs free energy of 1339 kJ/mol above the plateau (ca. 130 °C), reflecting its less sensitivity compared to F-2 under a continuous heating process. As a result, a lower temperature was required to drive the dehydration of the residual fraction of lower critical solution temperature (LCST) in nano-hybrid structures than TAP according to the results of DSC analysis. Thus, lower energy was expected to disintegrate the residual hydrogen bonds formed between the LCST chains and surrounding water molecules at elevated temperatures. Moreover, TAP-S formed a solid-micro-crosslinking structure network which exhibited a more stable hydrodynamic diameter as revealed by DLS analysis. Compared with TAP, TAP-S consisted of a larger composite B-SiNP-TAP integrated spatial network structure based on the results of environmental scanning electron microscope, which conferred a degree of thermal conductivity characteristic for improved temperature resistance. This contributed to the effective binding onto bentonite particles for protection and maintained a relatively stable bentonite particle dispersion according to the results of EPM and particle size distribution analyses. Consequently, TAP-S fortified drilling fluid demonstrates improved rheological and filtration performance under severe downhole conditions. Therefore, TAP-S, the thermo-associating copolymer integrated with B-SiNP could find potential application as an eco-friendly viscosifier in LSDFs for deep-well drilling operations.

© 2025 The Authors. Publishing services by Elsevier B.V. on behalf of KeAi Communications Co. Ltd. This is an open access article under the CC BY license (http://creativecommons.org/licenses/by/4.0/).

* Corresponding author.

Peer review under the responsibility of China University of Petroleum (Beijing).

1. Introduction

The inherent merits of bentonite clay such as cost attractiveness, desirable wellbore cleaning ability, and filtrate control ignite its preferential use in conventional water-based drilling fluids (WBDFs) (Oseh et al., 2019; Temraz and Hassanien, 2016). However,

^{**} Corresponding author.

E-mail addresses: towa2024@outlook.com (A.P. Tchameni), wxd8842@yeah.net (X.-D. Wang).

high content of bentonite clay in drilling fluids can compromise the fluid performance because of temperature-inducing clay flocculation and gelation under high-temperature and high-pressure (HTHP) conditions. This unwanted phenomenon causes excessive torque and drag, increasing chances of differential stuck pipe issues, decreasing the rate of penetration (ROP), and formation damage, which present a host of challenges during drilling operations (Li et al., 2018; Salami and Plank, 2016). Therefore, developing low-solid drilling fluids (LSDFs) is envisioned to exhibit a consistently predictable flow behavior and a higher quality mud filter cake, which are utmost desirable to inhibit formation damage under HTHP conditions.

Over the years, much attention was given to the substitution of bentonite clay with additives that impart an attractive thickening characteristic in aqueous solution. For most WBDFs, an exhaustive range of polymers could be used to mitigate the negative effect of bentonite clay while preserving satisfactory performance comparable to those of conventional drilling fluids. These polymers including biopolymers (xanthan gum, scleroglucan, and starches), chemically modified cellulose, and acrylamide-based polymers, among others have been reported to provide the desired rheological and filtration properties in WBDFs (Jain and Mahto, 2017; Li et al., 2015, 2016; Song et al., 2016b). However, the molecular chains of these polymers would adopt a random spiral conformation and even degrade when exposed to harsh conditions, leading to disastrous viscosity defects that affect the subsequent drilling process (Stamatakis et al., 2013; Tehrani et al., 2009). Although various stabilizing additives such as oxygen scavengers have been used to extend the thermal window, the lifespan of drilling fluids has not yet been significantly extended during deep-well drilling operations.

To overcome these inherent shortcomings, researchers have developed diverse functional polymers such as hydrophobically modified copolymers, super-high molecular weight polyacrylamide, temperature resistance modified polymers, amphoteric polymers, and comb-shaped polymers, etc., to improve the thermal, physical, and chemical properties of polymers over a certain ramp of conditions (Song et al., 2016a, 2016b; Zhong et al., 2022). Due to the low chemical and physical stability of the viscosity precursor under HTHP conditions, the thermal stability is still limited, leading to technical difficulties during drilling operations.

The oil and gas sectors have recently seen the advent of thermoassociating polymers as a viable contender to overcome the fatal viscosity fault of conventional polymers (Li et al., 2017; Ma et al., 2020; Tchameni et al., 2021b, 2024a, 2024b; Xie et al., 2023). The basic structure of this family of polymers consists of a hydrophilic backbone on which are grafted some few thermo-responsive sidechains (Guo et al., 2015; Petit et al., 2007b; Tchameni et al., 2021a) (characterized by a Lower Critical Solution Temperature, LCST) for temperature responsivity. The viscosity of typical polymers followed the Arrhenius relationship below the threshold temperatures (T_{cass}) ; however, when heated above the T_{cass} , thermoassociating polymers displayed an abrupt macroscopic behavior. This phenomenon was essentially linked to the switch of LCST precursors of thermo-associating polymers from hydrophilic character to hydrophobic character upon heating, which would induce a hydrophobic association effect and reinforce the network structure, and eventually the response in solution viscosity (Durand and Hourdet, 1999; Guo et al., 2015; Hourdet et al., 1994).

As previously reported, these appealing properties sparked interest in using thermo-associating polymers as efficient precursor viscosities for developing engineerable LSDFs to meet the technical challenges of the oil and gas industry (Xie et al., 2016; Xie and Liu, 2017). However, up to date, there are not only very limited works based on LSDFs that coped with HTHP conditions but also the

currently reported precursor viscosities are benzene-based polymers which display some level of toxicity and might pose a serious threat to the flora as a consequence to restrain their wide spectrum of applications (Xie et al., 2016; Xie and Liu, 2017). Therefore, exploring the feasibility of preparing a thermo-associating polymer with expanded temperature limitations while also mitigating the negative environmental impacts is urgently needed to develop technically reliable LSDFs, that are suitable for deep well drilling.

At present, there is a growing demand to develop materials with collective properties, which are not found in even one. The combination of materials with distinctive properties to acquire new products, generally known as "nano-hybrids" is perceived as a promising alternative in several industrial applications (Cao et al., 2018a, 2019; Li et al., 2024). It has been demonstrated that incorporating nanomaterials (NPs) into polymer molecular chains can result in a final product with micro-cross-linked structures that significantly improve thermal stability and mechanical properties under certain conditions (Martín-Alfonso et al., 2021; Zhang et al., 2021). These anticipated characteristics were ascribed to certain interactions between the host polymer and NPs (Cao et al., 2019; Zhu et al., 2014). Nano-hybrids are particularly of great interest where enhanced properties including flowability, wettability alteration, heat conductivity, and optical properties are requisite for the facile processability and flexibility of polymer structure, resulting in a material with exceptional chemical and thermal stability (Miranda et al., 2012; Roustaei et al., 2013). Literature is endowed with various nano-hybrids with an unrestricted range of NPs which have been incorporated into the molecular structures of polymers to improve the thermal stability, rheological and filtration loss properties of the drilling fluid, the thermal stability, reduce torque and drag, and maintain wellbore stability. These NPs include titanium dioxide (TiO₂) (Sadeghalvaad and Sabbaghi, 2015), zinc oxide (ZnO), copper oxide (CuO) (William et al., 2014), iron oxide (Fe₂O₃), silica (SiO₂) (Salih et al., 2016). Prominently reported among them, is silica nanoparticle (SiNP) because of its greater surface area, ordered structure, and advanced production process as well as its significantly beneficial impact on the rheological and filtration loss properties of WBDFs (Salih et al., 2016; Xie et al., 2023; Cao et al., 2018b, 2019). Xie et al. (2023) exploited the synergistic effect between the thermo-associating polymer (CGBA) and SiNP to develop an organic/inorganic hybrid system that enhanced the rheological properties (AV, PV, and YP) of bentonite-free drilling fluid by about 16-fold compared to CGBA-bearing bentonite-free at 200 °C. Mao et al. (2015) proposed a hydrophobic-associated polymer-based SiNP composite with a core-shell structure that could not only improve the HTHP filtration loss and rheological properties of drilling fluid at 230 °C, but also showed certain tolerance to saline-alkaline environments. Wandji Djouonkep et al. (2024) reported on an amphoteric polymer nanocomposite (Nano-DAVD) with SiNP that did not remarkably only better control the filtration loss properties of WBDF in the presence of 15% NaCl but also improved the quality of the mud filter-cake compared to the free-SiNP polymer counterpart at 240 °C. Additionally, the authors also found that Nano-DAVD slight improvement in the rheological properties at high temperatures (Djouonkep et al., 2024). Liu et al. (2021) did a study on the polymer with a core-shell structure based on SiNP as a filtration loss reducer (NS-DA) in WBDFs. They reported that when NS-DS was added to the drilling fluid, its filtration loss volume was favourably as low as 5.6 mL at 180 °C, which was far better than that of some commercial filtrate reducers (such as Driscal D, PAC-Lv, and CMC) under the same conditions. Another relevant study done by Pang et al. (2025) revealed a zwitterionic polymer nanocomposite (AAND-S) based on SiNP acting as a filtrate reducer in WBDFs at high temperatures. They observed that AAND-S did not only reduce the filtration loss volume of the base fluid

from 44 to 12.25 mL but also demonstrated favorable tolerance to sodium chloride contamination up to 25% at 220 °C. Leveraging on the extraordinarily charming and beneficial aforementioned properties, there are versatile synthesis routes to produce a variety of nano-hybrid structures that unify thermo-associating polymers such as poly(N-alkylacrylamide) and polyethers through interaction with the surface of SiNP to form a nano-hybrid network with viscoelasticity comparable to chemical gels (Sanchez et al., 2005; Petit et al., 2007a; Vallejo et al., 2019).

Extraction of silica from agricultural waste is attracting paramount attention as it could be perceived as a more environmentally and economically sustainable strategy for broad ramp of industrial applications than commercial SiNPs which not only demonstrate some level of toxicity but also require high operational cost and stringent synthesis conditions. In recent years, exhaustive studies have tended to focus on the extraction of biogenic-nanosilica in rice husks (RHs) attributed to its high content compared to other agricultural disposed waste (Keshavarz Moraveji et al., 2020; Liou, 2004; Okon et al., 2014). Thus, RHs can be used as raw materials to extract amorphous or crystalline SNPs based on the annealing temperatures (Umeda and Kondoh, 2010). The nanomaterials (ca. biogenic-SiNPs) are gradually attracting special interest for technologically innovative solutions in the petroleum sectors (Gautam and Guria, 2020; Umeda and Kondoh, 2010). Raipuria et al. (2018) demonstrated that the biogenic-SiNPs were almost as effective compared to the traditional SiNP in terms of controlling the rheological flow and filtration loss properties in drilling fluids at high temperatures (Raipuria et al., 2018). Owing to their uniform dispersion and defined morphology, the biogenic-SiNPs enhanced the oil recovery efficiency by roughly 5%-7% relative to the traditional SiNPs (Zamani et al., 2020). However, as the biogenic-SiNPs (B-SiNPs) display identical inherent characteristics to that of the commercial SiNPs, their dispersion state might be compromised under harsh environmental conditions, which thus erects the necessity of surface modification of optimal nanodispersion.

Given the possibility of polymer molecules binding to the surface of nanomaterials, we used vinyl triethoxysilane (VTES) to modify the surface of B-SiNPs, which was prepared by our research team (Tchameni et al., 2025) and then synthesized the thermoassociating polymer nano-hybrid materials (TAP-S) by in-situ free-radical polymerization technique. The molecular structure of TAP-S was designed as follows: AMPS monomer which had been widely employed in oilfield operations for its attractive thermal and hydrolytic stability, and high reactivity was chosen to afford a relatively rigid copolymer molecular chain; thermos-sensitive monomer NVCL, whose corresponding polymer (PNVCL) solution segregate into two distinctive phases when heated above the LCST (ca. around 32 °C), was used to improve the rigidity of the polymer molecular chain and increase the viscosifying properties and structural strength of polymer in drilling fluids at high temperature; cross-linking monomer MBA was employed to afford polymer conformation with micro-crosslinkages to improve the viscosity and structural strength; vinyl-terminated biogenic nanosilica (VB-SiNPs) was incorporated to reinforce the micro-crosslinked structure and improved the temperature conductivity characteristic of the polymer. Meanwhile, a thermo-associating polymer (TAP) was also prepared as a control sample under the same conditions. In each case, we investigated the feasibility of incorporating B-SiNP into the molecular skeleton of TAP with respect to the fluid rheological controlling ability at HTHP conditions. In relation to the macroscopic properties of the fluids, the DSC, DLS, ESEM, EPM, particle size distribution, and SEM were used to elucidate the distinctive mechanisms driving rheological controlling ability in LSDF under deep well drilling operations. For the first time, the feasibility of incorporating B-SiNPs into the molecular skeleton of the thermo-associating polymer was explored in this study as a high-performance eco-friendly, and economically viable precursor viscosity in LSDFs for optimal performance during deep well drilling operation.

2. Experimental

2.1. Materials

Based on previous work, the B-SiNPs with an average particle size in the range of 25–45 nm, and a specific surface area of 525 m^2 / g with a total pore volume of 1.13 cm³/g were extracted from rice husks via the sol-gel method (Tchameni et al., 2025). The reagents used for the extraction were as follows, husks (RHs) acquired from a rice mill in Wanzhou in Chongqing (China), sodium hydroxide (NaOH), sodium sulfite (Na₂SO₃, 98%), sodium carbonate (Na₂CO₃, 98%), anhydrous ethanol (EtOH) and hydrochloric acid (36%–38%) were from Tianjin Beilian Fine Chemicals Development Co. Ltd. Nvinylcaprolactam (NVCL, 98%), 2-acrylamido-methylpropane sulfonic acid (AMPS, 99%), vinyl triethoxysilane (VTES, 98%), 2,2'azobis[2-(2-imidazolin-2-yl)propane]dihydrochloride (AIBI, 99%), N,N'-methylenebis (acrylamide) (MBA, 99%), trimethylamine (TEA, 99%), and sodium montmorillonite (Mt) were all acquired from Shanghai Macklin Biomedical Co. Ltd. The bentonite which was according to the API standard as well as calcium carbonate (CaCO₃), and DSP-1 were procured from Jingzhou Jiahua Technology Co. Ltd. In all the tests, the electric heating water distiller (Biobase Meihua Trading, Model WD-A20) was used for the distillation of water.

2.2. Synthesis methods

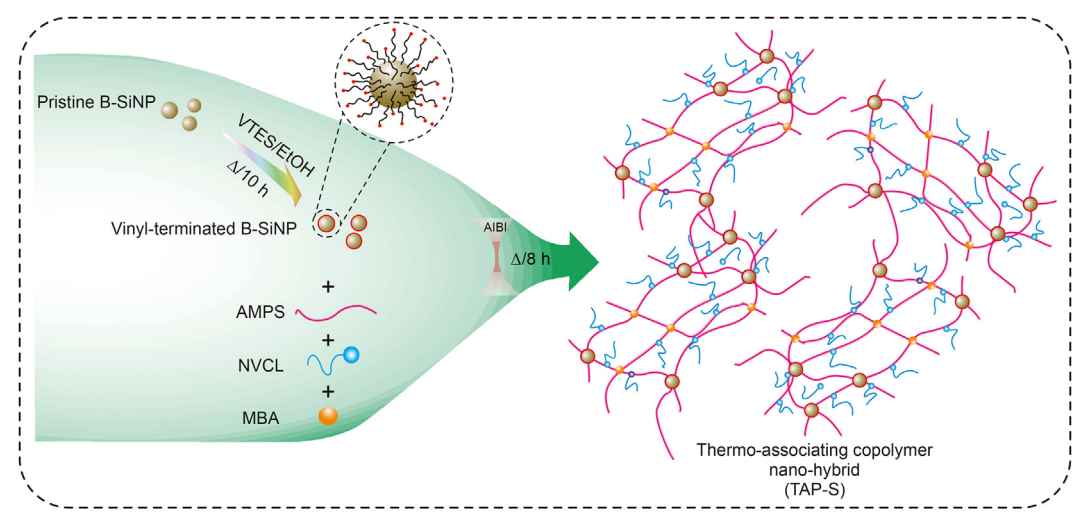
B-SiNP-TAP was prepared based on a two-step reaction as schematically illustrated in Scheme 1.

2.2.1. Synthesis of vinyl-terminated B-SiNP (VB-SiNP)

The surface modification process for B-SiNP was adapted from a procedure proposed by Cao et al. (2018a). In detail, dried SiNP (4 g) was first dissolved in EtOH (100 mL) with a pH value controlled to 8 using TEA. After 60 min of intensive ultrasonication at ambient temperature, a desired amount of VTES contained in a small volume of EtOH was added dropwise to B-SiNP/EtOH dispersion and mixed evenly. The reaction was carried out at 85 °C for 10 h under refluxing. VB-SiNP was recovered by centrifugation after repeated washing with EtOH at least four times to remove the unreacted coupling agents and TEA (4000 rpm for 30 min, at ambient temperature), and oven-dried overnight. A series of VB-SiNP based on the distinctive content of VTES were prepared in this study and their parameters are compiled in Table 2.

2.2.2. Synthesis of thermo-associating copolymer nano-hybrid materials

A series of nano-hybrid materials were prepared by in-situ polymerization in distilled water using comonomers of NVCL, AMPS, and MBA. At room temperature, the comonomers were mixed with the nanomaterials priorly intensively ultrasonicated in a small volume of EtOH to attain a total monomers concentration of 10 wt% and the pH value was controlled between 8 and 9 using a concentrated NaOH solution. The mixture was then stirred in a three-necked flask equipped with an electric stirrer under a nitrogen atmosphere for 1 h and the reaction temperature was controlled with a thermostatic water bath. Subsequently, a degassed stock solution of AIBI (1 wt/v% based on the total mass of comonomers) was introduced to the mixture to induce the polymerization and the reaction was left to proceed under continuous nitrogen injection at the reaction temperature for 8 h. After the



Scheme. 1. Two-step reaction of TAP-S.

Table 1 Composition of LSDFs.

Additive	Function	Concentrati	on, wt%	
		F-1	F-2	F-3
Tap water	Continuous phase	400	400	400
Bentonite clay	Viscosifier	3	3	3
FC-Amihib	Shale inhibitor	3	3	3
Fine CaCO ₃	Filtration loss reducer	3	3	3
DSP-1	Filtration loss reducer	1	1	1
TAP	Viscosifier	/	1.5	1
TAP-S	Viscosifier	/	/	1.5
Na_2SO_3	Oxygen scavenger	0.5	0.5	0.5
Barite	Weighting agent	As needed	As needed	As needed

reaction, the viscous solutions were repeatedly washed with a large volume of acetone/water (v/v, 4/1), and then freeze-dried to obtain the target products. TAP, which refers to thermo-associating copolymer free-B-SiNP was also synthesized under identical conditions for comparison. The chemical structure of TAP-S is indicated in Fig. 1.

2.3. Characterization of nanomaterials and nano-hybrid materials

FT-IR analysis was performed on an FT-IR 650 (Tianjin, China) in the frequency range of 4000–400 cm $^{-1}$. Elemental analysis (C, H, S, and N) was carried out on the Vario Micro 28 cube elemental analyzer. The thermal stability was tested on a Pyris 1 thermogravimetric analyzer with a heating rate of 10 °C/min from room temperature to 900 °C under $\rm N_2$ gas. The morphology of nanomaterials was observed by transmission electron microscopy (TEM)

(JEM-2100UHR, JEOL, Japan). The particle size was examined by collecting aliquots of nanodispersions whose variation in particle size was studied on a particle size analyzer (BT-9300LD, Betttersize, Shanghai, China). The specific surface area of the nanomaterial was studied through Brunauer-Emmett-Teller (BET) (Autosorb AS-1 MP Surface area and pore size analyzer, USA) using nitrogen adsorption and desorption techniques. The colloidal stability of the nanodispersions was further tracked using the Formulaction Turbiscan LAB (MA 2000, France). In all the tests, the measurements were taken in triplicate and averaged to obtain the final results.

2.4. Application of thermo-associating polymer nano-hybrid in LSDF

2.4.1. Sample preparation

A low-fresh solid slurry was prepared by mixing bentonite clay, Na₂CO₃, and tap water (3:0.5:100 ratio by weight), and allowed to pre-hydrate for 24 h at ambient temperature. Subsequently, all the additives listed in Table 1 were added sequentially to the slurry under mechanical stirring at 3000 rpm for 20 min to formulate the LSDFs. F-1 was considered as the base fluid, providing information on the thermo-stability of the prepared drilling fluid while F-2, and F-3 containing TAP and TAP-S, respectively, previously synthesized in-situ, following the procedure provided in Section 2.2, were prepared in the descending order of the formulations. The thermal stability of the formulated fluid samples was monitored by the hotrolling process at different temperatures (ca. 170, 200, 230 °C) up to 230 °C to simulate the bottom hole temperature in the buried hill field in Jidong Oilfield of Bohai Sea Bay Basin which can reach 220 °C (Mao et al., 2016).

Table 2 Physicochemical parameters of nanomaterials.

Sample	SiNP, g	VTES, g	Mole ratio of -OH/VTES	Elemer	ital analys	is	Vinyl group density, mmol/g ^a	Specific surface area, m ² /g ^b
				C, %	H, %	N, %		
VB-SiNP-1	4	0.8	1:1	3.46	1.44	0.21	0.53	525
VB-SiNP-2	4	1.2	1:2	4.07	1.81	0.20	1.03	555
VB-SiNP-3	4	1.6	1:4	5.12	1.91	0.22	1.85	590
VB-SiNP-4	4	2.0	1:8	4.23	1.65	0.23	1.71	585

a Determined by elemental analysis.

^b Estimated by BET analysis.

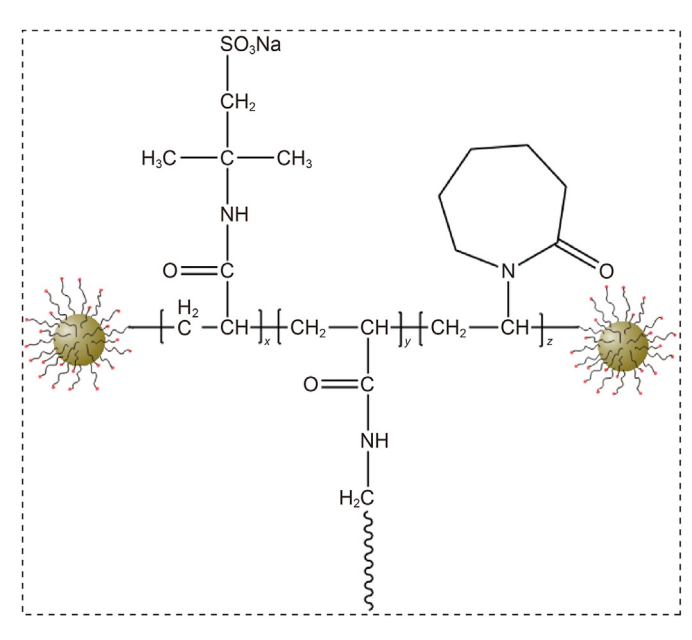


Fig. 1. Chemical structure of TAP-S.

2.4.2. Rheological measurement

Two types of viscometers were used to examine the viscosity of the fluid samples. First, the fluids were hot-rolled (OFI Testing Equipment, US) at set temperatures for 16 h, then cooled to room temperature. Subsequently, the rheological parameters including, the apparent viscosity (AV), plastic viscosity (PV), yield point (YP), and gel strengths (ca. 10-min and 10-sec gel strengths) were determined from the dial readings at a rotor speed of 600 rpm and 300 rpm viscometer readings taken using ZNN-D6B six-speed rotary viscometer (Qingdao Shande Petroleum Instrument, China) based on API 2009 guideline 13B-1 for field testing of water-based drilling fluids (API Recommended Practice, 2009).

A Physica MCR 302 (Anton Paar) rotational rheometer equipped with Searle-type concentric cylinder geometry was used for both shear viscosity and oscillatory rheological measurements at distinct temperatures. The measurements were conducted between 25 and 210 °C at a fixed shear rate of 10 s⁻¹. The heating runs were performed at 5 °C/min with the necessary precautions to ensure repeatability and reproducibility. The dynamic moduli parameters (G' and G'') of the fluids were also recorded by monitoring the stress and using concentric cylinder geometry. Before taking the measurements, the strain amplitude was adjusted to make sure that the test was conducted in a linear viscoelastic regime at temperatures of 25, 170, 200, and 230 °C. In addition, the shear steady viscosity (η), normal stress (N_1), and relaxation time (θ) were also determined.

2.4.3. Filtration control test

The standard filtration loss properties of the fluids were determined at ambient temperature and 0.7 MPa with a nitrogenapplied medium pressure apparatus while the HTHP filtration loss was carried out at a temperature of 180 °C and pressure of 3.5 MPa in compliance with API 2009 guideline 13B-1 (API Recommended Practice, 2009). Besides noting the filtration volumes, the filter cakes were vacuo-dried, and the surface micromorphology was observed by a Zeiss Gemini SEM-HRSEM. All the apparatus used for the tests were supplied by Qingdao Haitongda Specialized Instrument Company.

2.5. Regulation of fluid rheological properties

2.5.1. Differential scanning calorimetry experiments

The phase segregation was tracked by Netzsch Differential scanning calorimetry (DSC) 204 F1 Phoenix analyzer in the temperature range between 20 and 90 °C at a heating rate of 1 °C/min. The endothermic peak could be integrated to obtain the cumulated enthalpy (H) using the temperature dependence of the heat flow. Subsequently, the transition enthalpy per mole of repeating units of NVCL (ΔH) was taken as the higher value of this cumulated enthalpy (H).

2.5.2. Dynamic light scattering (DLS) measurement

The hydrodynamic diameter of nano-hybrid materials in an aqueous solution was determined using a Multi-detector light scattering unit (DAWN HELEOS, Wyatt Technology Corporation, US).

2.5.3. Environmental scanning electron microscope test

The microscopic morphology of nano-hybrid materials in aqueous solutions was visualized by environmental scanning electron microscope (FEI ESEM Quanta 450) as per the previous reports (Chen et al., 2013; Tchameni et al., 2021a).

2.5.4. Electrophoretic mobility (EPM) measurement

Malvern Instruments Zetasizer Nano Z was employed to investigate the effect of polymeric materials on the EPM of Mt fluids, and the concentration of the sample was set at 0.1 wt/v% with a pH value adjusted to 8 using NaOH.

3. Results and discussion

3.1. Characterization of nanomaterials

A series of vinyl-terminated B-SiNP based on the distinctive content of the coupling agent (ca. VTES) was first prepared via surface modification in EtOH, and the molecular structural characterization was conducted using elemental analysis, particle size measurement, wettability, EPM, FT-IR, and TEM analyses.

3.1.1. Elemental analysis, particle size distribution, and wettability

As can be seen in Table 2, the optimal vinyl deposition layers onto the B-SiNP surface were obtained as 1.85 mmol/g (ca. VB-SiNP), which is prominently higher than that reported in previous works (Cao et al., 2018a; Xie et al., 2023), presumably ascribed to a prolonged reaction time, which contributed to the deposition of a thicker vinyl multi-layers (Vandenberg et al., 1991). The deposition of vinyl groups onto the surface of B-SiNP increased proportionally with the feed amount of VTES, and monotonically attained saturation at 1:4. Further increase in the VTES feed amount (ca. 1:8) compromised the deposition layer, which is consistent with a previous study (Zhao et al., 2012; Traciak and Żyła, 2022). In our previous work, the particle size of B-SiNP ranged from 25 to 45 nm, but surprisingly, it increased to 245 nm presumably due to strong flocculation propensities in aqueous medium. Nevertheless, as indicated in Fig. 2(a), the particle size gradually reduced with increasing VTES feed amount, suggesting better dispensability, which corroborated the findings of the specific surface area. The electrical potential was examined by tracking the electrophoretic mobility (EPM) of the nanodispersion with respect to feed amount of VTES as presented in Fig. 2(b). It was obvious that the deposition of the coupling agent induced a more negatively charged surface up

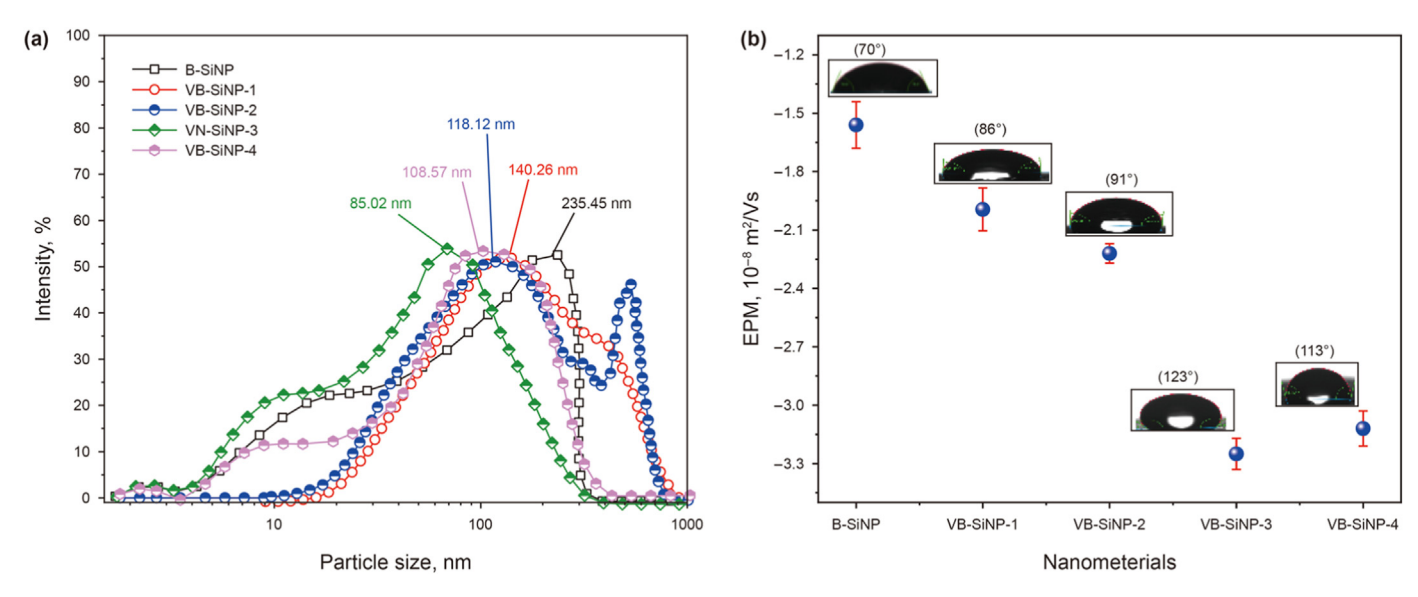


Fig. 2. (a) Particle size distribution and (b) EPM of nanomaterials.

to the optimal value at VB-SiNP-3, which was also indicative of the surface saturation under the investigated conditions. Simultaneously, the surface hydrophobicity of B-SiNP was reinforced as indicated in the inset Fig. 2(b). Further increase in the feed amount of VTES (ca. VB-SiNP-4) led to a gradual diminution of the EPM as well as the contact angle, which could irreversibly promote nanodispersion stability defect as VTES could not transcend the saturation limit (Traciak and Żyła, 2022).

3.1.2. FT-IR analysis

FT-IR spectra of B-SiNP, and vinyl-terminated B-SiNP are shown in Fig. 3. The broad peak at 3411 cm⁻¹ was due to O—H stretching vibration from B-SiNP and VB-SiNP. Compared to B-SiNP, several new peaks appeared on the surface of vinyl-terminated B-SiNP. The peak around 2912 cm⁻¹ which is attributed to the C—H stretching vibration of the coupling agent became prominent with increasing

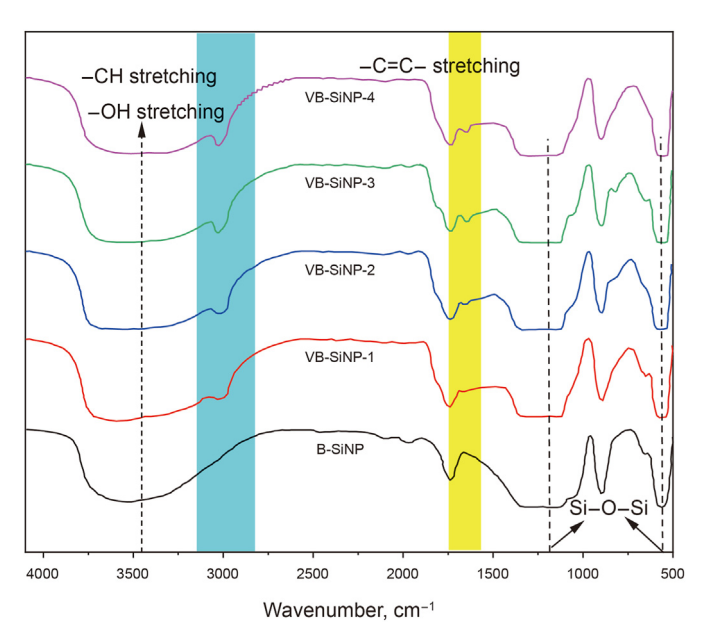


Fig. 3. FT-IR of nanomaterials.

feed amount in the VTES. Similarly, the characteristic peak at 1593 cm⁻¹ was attributed to the C=C vibration of VTES. For all the nanomaterials, the asymmetrical stretching of Si-O-Si vibrated at 1111 and 477 cm⁻¹ (Al-Oweini and El-Rassy, 2009).

3.1.3. TEM analysis

The morphologies of B-SiNP, vinyl terminated B-SiNP dispersed in distilled water were visualized by Transmission Electron Microscopic (TEM), as depicted in Fig. 4. It can be observed that B-SiNP was more intensely aggregated than VB-SiNP, which exhibited a comparatively loose structure and slightly uniform dispersion. After the silanization process of B-SiNP, the surface energy between the particles is reduced driving weakening effect of van der Waals interactions, which causes the aggregation tendency (Guo et al., 2008).

3.2. Colloidal stability

In this subsection, the long-term colloidal stability of the nanomaterials with respect to surface modification was studied with emphasis on the proper integration of the nanomaterials into the copolymer molecular architecture for improved thermalconductivity characteristics, to ultimately extend the thermal resistance of working fluids. Preliminary results on comparative colloidal stability between the B-SiNP and series of vinylterminated B-SiNP via visual observation over 10 days in distilled water at neutral conditions (ca. pH 7) are indicated in Fig. 5(a). The nanomaterials maintained a certain dispersion in distilled water on the first day as no obvious sign of sedimentation was noticed. However, the VB-SiNP demonstrated better dispersion as the solutions were more transparent than the parent B-SiNP, which could be ascribed to the random motion of nanoparticles in the dispersed aqueous medium (ca. so-called Brownian motion) as VB-SiNP reached equilibrium under the investigated conditions (Harish and Sivakumar, 2021; Hayat et al., 2017). From the same figure, it is obvious that B-SiNP underwent sedimentation after 5 days and the dispersed medium became totally transparent. A similar observation was made for VB-SiNP-1 nanodispersion as strong flocculation tendencies arising from the hydroxyl groups governing the system and contributing to their partially wetting characteristics after 10 days (which was obvious earlier in the wettability

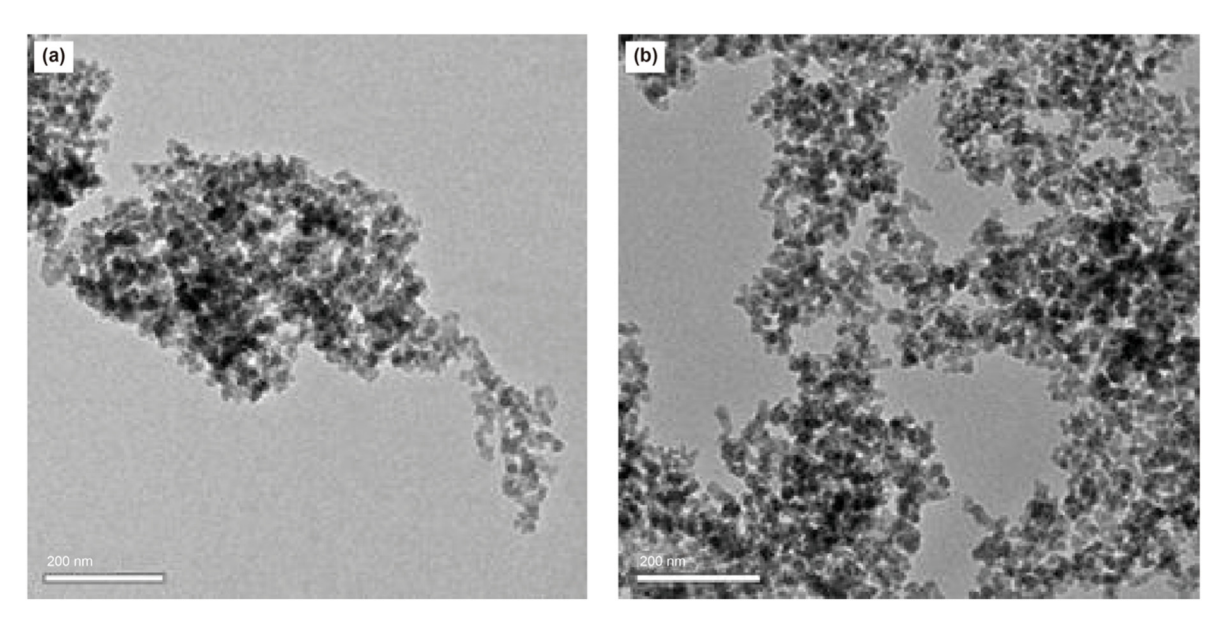


Fig. 4. TEM of nanomaterials dispersed in distilled water. Note: (a) B-SiNP and (b) VB-SiNP-3.

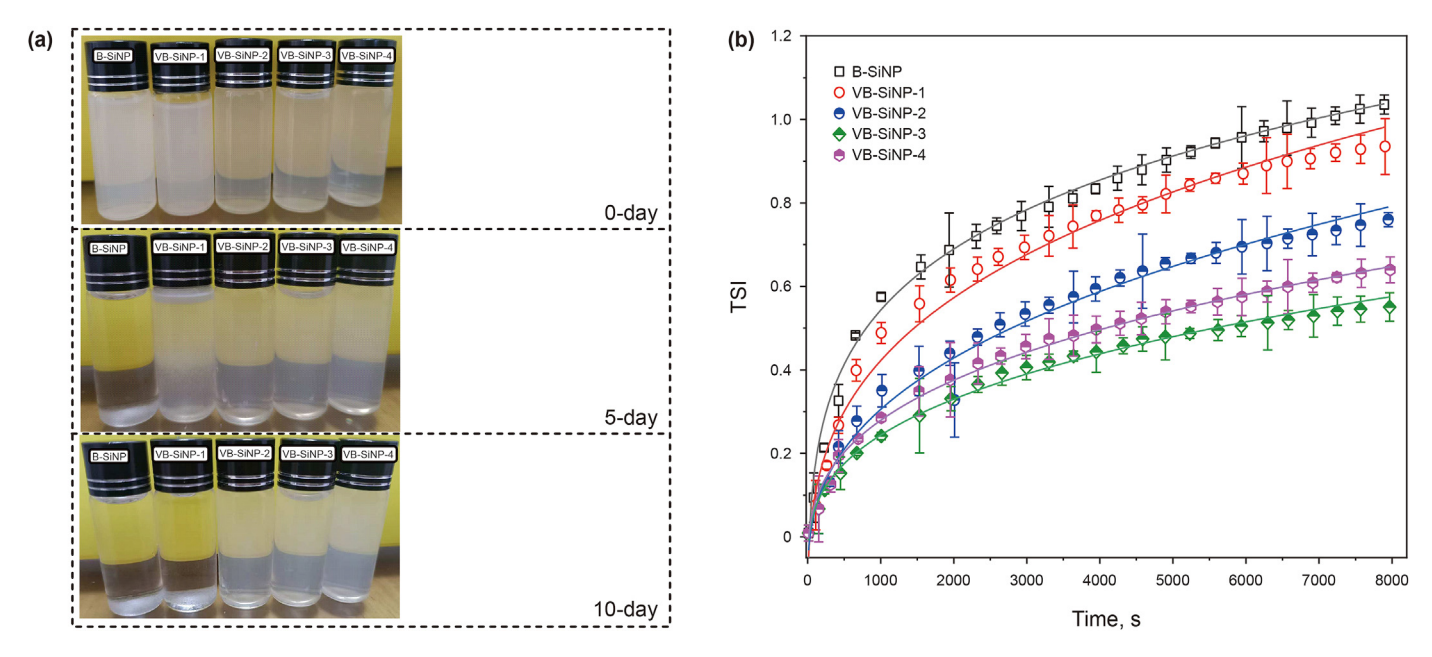


Fig. 5. Colloidal stability of nanomaterials: (a) Photographs of nanomaterials dispersed in distilled water; (b) TSI of nanomaterials.

analysis). Comparatively, VB-SiNP-2, VB-SiNP-3, and VB-SiNP-4 nanomaterials apparently maintained relative stability over 10 days and it was quite uncertain to precisely characterize their colloidal stability through visual observation. For this purpose, the colloidal stability of the nanodispersions was intuitively tracked using the Turbiscan stability index (TSI), whose quantity is conversely proportional to the stability of materials, and the results are presented in Fig. 5(b). As observed, the deposition of VTES noticeably influences the colloidal stability of the nanodispersion with reference to the corresponding TSI. B-SiNP had the fastest increasing rate of the TSI followed by VB-SiNP-1 and VB-SiNP-2, inferring that the nanomaterials gradually lost their stability due to their low hydrophobic characteristics. The lowest TSI of VB-SiNP-3 (ca. 0.55), indicates its favorable stability and hydrophobic character over time. Further increases in VTES feeding amount (ca VB-

SiNP-4) compromised the deposition of thicker vinyl multi-layers owned to unwanted cross-linking processes, which favored not only a high chance of electrostatic instability but also nanomaterial sedimentation, and ultimately increased TSI (ca. 0.67). The favorable colloidal stability demonstrated by VB-SiNP-3 was consistent with the results of the wettability testing, therefore, this nanomaterial was selected for subsequent synthesis experiments.

- 3.3. Synthesis and characterization of thermo-associating polymer nano-hybrid TAP-S
- 3.3.1. Synthesis of thermo-associating copolymer nano-hybrid TAP- $\ensuremath{\mathsf{S}}$

Nanosilica-hybrid material TAP-S was prepared based on the two-step reaction as illustrated in Scheme 1. The products were

prepared by in-situ polymerization using comonomers of AMPS, NVCL, and cross-linking MBA in distilled water in the presence of AIBI. During the synthesis reaction, the key factors including monomers feed ratio, content of nanomaterials, reaction temperature, and reaction time were found to prominently influence the performance efficiency of the target products. Therefore, an orthogonal array L₉ (3⁴) was designed for the optimization of the synthesis process. The key factors and levels of this synthesis reaction are listed in Table 3. As the characterization of rheological properties of drilling fluids implied the identification of the key parameters including apparent viscosity (AV), plastic viscosity (PV), and yield point (YP), the optimal synthesis conditions were identified according to the YP which refers to the amount of tension necessary to initiate deformation in the drilling fluids to initiate its flow whereas YP/PV ratio which denotes the shear-thinning behavior as an index of drilled-cuttings transport. As stated in our previous work (Xie et al., 2023), these two key parameters were normalized (denoted YP and YP/PV as X and Y, respectively). Subsequently, an identical weight fraction was applied to these two rheological properties indicators. Specifically, the level of variation in properties of the slurry was calculated by the relationships given in Eqs. (1)-(3)

$$X = \frac{(YP - YP_{min})}{(YP_{max} - YP_{min})}$$
(1)

$$Y = \frac{\left[(YP/PV) - (YP/PV)_{min} \right]}{\left[(YP/PV)_{max} - (YP/PV)_{min} \right]}$$
(2)

$$Z = X + Y \tag{3}$$

The bigger the X value, the greater the YP and YP/PV ratio would be for satisfactory fluid flow. In the course of the investigation, a prehydrated low bentonite slurry (3 wt%) was incorporated with 1 wt% nanocomposite and 0.5 wt% oxygen scavenger Na_2SO_3 and the key rheological indexes were collected after the hot-rolling processes at 230 °C for 16 h.

Albeit the poor *Z* values, which reflect the instability of drilling fluid samples (see Table 4) mainly attributed to the gradual

molecular deterioration of the polymeric material under the continuous hot-rolling procedures. However, varying the key factors could potentially improve these values. Among the key factors, the comonomers feed ratio had the most significant impact on the optimization process. Based on the mean analysis findings, TAP-S was prepared using the optimal synthesis conditions of AMPS/ NVCL/MBA = 55:45:0.7, the weight fraction of nanomaterial = 4 wt/v, reaction temperature = $50 \, ^{\circ}\text{C}$, and reaction time = $8 \, \text{h}$. For comparison purposes, the thermo-associating polymer free-nanomaterial (ca. TAP) was synthesized under the same conditions.

3.3.2. Characterization of thermo-associating copolymer nanohybrid TAP-S

3.3.2.1. FT-IR and 1H -NMR spectra. The molecular structure of TAP and TAP-S were proved using FT-IR as shown in Fig. 6(a). The spectra of TAP showed adsorption peak characteristics as follows; the stretching vibration of $-CH_2$ appeared around 2977 cm $^{-1}$. The stretching vibration of C=O contributed to the peak at 1720 cm $^{-1}$. The bending vibration absorption of -CH, $-CH_3$, and $-CH_2$ were attributed to the peaks detected between 1338 and 1491 cm $^{-1}$. The adsorption peaks at 1212 cm $^{-1}$ were due to the stretching vibration of $-SO_3^-$. Considering the nano-hybrid material TAP-S, in addition to all the adsorption peaks characteristic of TAP, the key adsorption peaks of silicate groups appeared at 883 and 493 cm $^{-1}$ associated with the S-O stretching and bending vibration, respectively (da Luz et al., 2019).

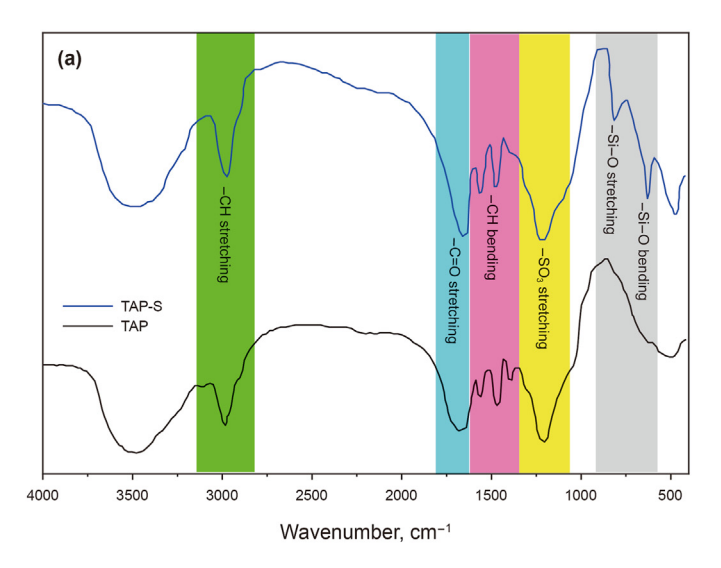
The molecular structure of TAP-S was further elucidated by 1 H-NMR as indicated in Fig. 6(b). It can be readily seen that TAP and TAP-S had a similar spectrum. Briefly, the hydrogens in the $-CH_{2}(l)$ of NVCL units appeared at 1.12 ppm. The hydrogens of $[-(CH_{3})_{2}C-]$ (b) in AMPS units and those in the $-CH_{2}(m,k)$ of NVCL units were assigned to the peak at 1.47 ppm. The signal between 2.16 and 1.99 ppm was due to the hydrogens in -CH and $-CH_{2}$ of the central chain (c, d, e, f, h, i). The peak detected between 2.01 and 2.61 ppm was attributed to the hydrogens in the $-CH_{2}(j, n)$ of the NVCL units. The hydrogens in $-CH_{2}(a)$ in the AMPS units and those $-CH_{2}(k)$ in the NVCL units were detected at 3.31 ppm. The hydrogens in $-CH_{2}(g)$ of MBA cross-linking were due to the peak at 3.32 ppm. The peak between 7.43 and 7.62 ppm corresponded to the vinyl protons anchored to the surface of B-SiNP. The recorded peaks emerging

Table 3Factors and levels of Orthogonal test array to fabricate the nanocomposite.

Factor level	Comonomers feeding ratio AMPS/NVCL/MBA, mol%	Content of nanomaterial, wt%	Reaction temperature, °C	Reaction time, h
Level 1	45:55:0.7	3	40	6
Level 2	50:50:0.7	4	45	7
Level 3	55:45:0.7	5	50	8

Table 4Orthogonal test array results of nanocomposites.

Sample	Comonomers feeding ratio AMPS/NVCL/MBA, mol%	Content of nanomaterial, wt%	Reaction temperature, °C	Reaction time, h	YP, Pa	YP/PV ratio	Z
1	45:55:0.7	3	40	6	6	0.17	0.050
2	45:55:0.7	4	45	7	7.5	0.29	0.47
3	45:55:0.7	5	50	8	8	0.37	0.51
4	50:50:0.7	3	45	7	7	0.26	0.41
5	50:50:0.7	4	40	8	9.5	0.50	0.60
6	50:50:0.7	5	50	6	7	0.25	0.43
7	55:45:0.7	3	50	6	8.5	0.40	0.53
8	55:45:0.7	4	45	8	9	0.45	0.57
9	55:45:0.7	5	40	7	8	0.36	0.50
K_1	0.343	0.330	0.383	0.337			
K ₂	0.480	0.546	0.483	0.460			
K ₃	0.553	0.480	0.490	0.547			
R	0.459	0.452	0.452	0.448			



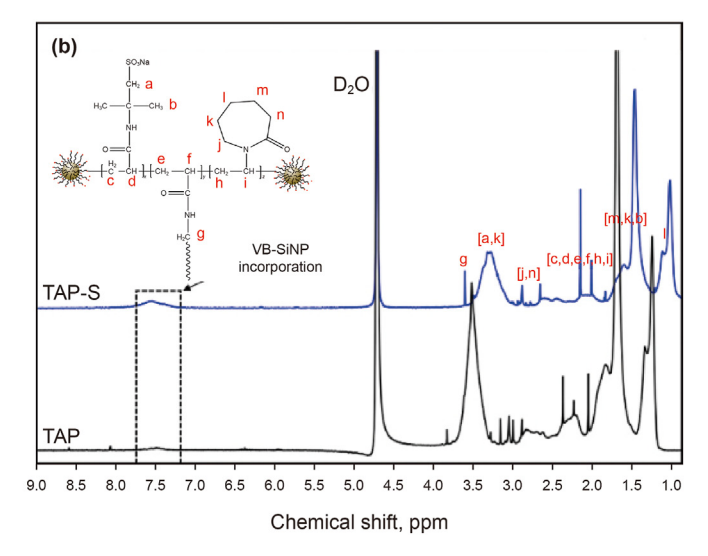


Fig. 6. (a) FT-IR and (b) ¹H-NMR spectra of polymeric materials.

Table 5Nomenclature of TAP and TAP-S

Sample	Initial feed ratio of A	MPS/NVCL/MBA, wt% ^a Content of nanomateria	ls, wt% Elemental and	alysis	The final feed ratio of AMP	S/BA/DVB, wt% ^b Grafting ratio. wt% ^c
	_	_	C, wt% N, wt%	S, wt%	6	
TAP	55:45:07		36.15 7.31	6.42	62.43:36.75:0.52	73.50
TAP-S	50:45:0.7	4	32.78 6.47	6.05	62.90:36.45:0.55	72.90

- ^a Initial mass percentage of comonomers.
- ^b Determined by elemental analysis.

from TAP-S and TAP proved their chemical structure and undoubtedly evidenced the successful integration of the nanomaterial into the skeleton of TAP.

3.3.2.2. Elemental analysis. The results of the elemental analysis are listed in Table 5. Interestingly, it was noticed a slight variation in the actual mole ratio of AMPS, NVCL, and MBA for both copolymers. These findings were consistent with those of ¹H-NMR, inferring that the addition of nanomaterials in bulk polymerization had a minimal impact on the reactivity of monomers, and were consistent with a previous report (Cao et al., 2018a).

3.3.2.3. TGA analysis. The thermal behavior of TPA and TAP-S are indicated in Fig. 7(a). The two samples presented three stages of weight loss upon heating. When heated up to 220 °C, all the samples exhibited almost identical weight loss attributed to the elimination of free water adsorbed from the environments (Tchameni et al., 2021b). The second stage of decomposition of TAP occurring between 220 and 310 °C with a weight loss of 15.78% was attributed to the degradation of sulfonyl groups, and the third stage was over 311 °C. However, unlike TAP, the decomposition of the TAP-S counterpart occurred at a relatively higher temperature with a threshold thermal stability observed between 220 and 348 °C with a weight loss of almost 16.60%. Further increase in temperature prompted remarkable stepwise decarboxylation of carboxylate functional groups and cleavage of C-N and C-C linkages above 350 °C. The DTG thermogram shown in Fig. 7(b) clearly confirmed the main decomposition temperatures of TAP and TAP-S were at 310 and 348 °C, respectively.

3.4. Properties evaluation of TAP-S fortified LSDFs

Optimal drilling fluids properties are fundamentally necessary, especially, for efficient and safe drilling operations of depth wells. The key parameters of drilling fluids including density, rheological, and filtration loss properties were used to examine the effect of integrating B-SiNP into the molecular structure of thermoassociating copolymer TAP with respect to drilling fluid performance.

3.4.1. Rheological properties

The rheological stability of the drilling fluid samples fortified with polymeric materials was examined by hot rolling at elevated temperatures (ca. 170, 200, and 230 °C), and then cooled to room temperature, and key parameters were measured. Results of the rheological parameters (ca. AV. PV. YP. and Gel strengths) of the drilling fluid samples are shown in Fig. 8(a) and (b). The drilling fluids exhibited interesting characteristics in retaining their rheology albeit their efficiencies decreased with rising oventreatment temperatures. The F-1 exhibited the lowest rheological properties throughout the investigated temperature range, which was expected for a polymer-free drilling fluid sample. The F-2 lost almost 50% of its initial viscosity at 170 °C, and the AV prominently diminished by almost 80% with increasing oven treatment up to 230 °C as indicated in Fig. 8(a), mainly because of deterioration of TAP molecules caused by the exposure to prolonged hot-rolling treatment for 16 h. This explanation may be connected to the drastic drop in the PV and YP (Fig. 8(a)), and Gel strengths (Fig. 8(b)). The rheological properties of TAP-S fortified fluids shown in Fig. 8(a) and (b) indicate relative stability at 200 °C as it almost retained 90% of their initial fluid properties (ca. AV, PV, and

^c Determined from the ratio final feed ratio of NVCL to the initial feed ratio of NVCL.

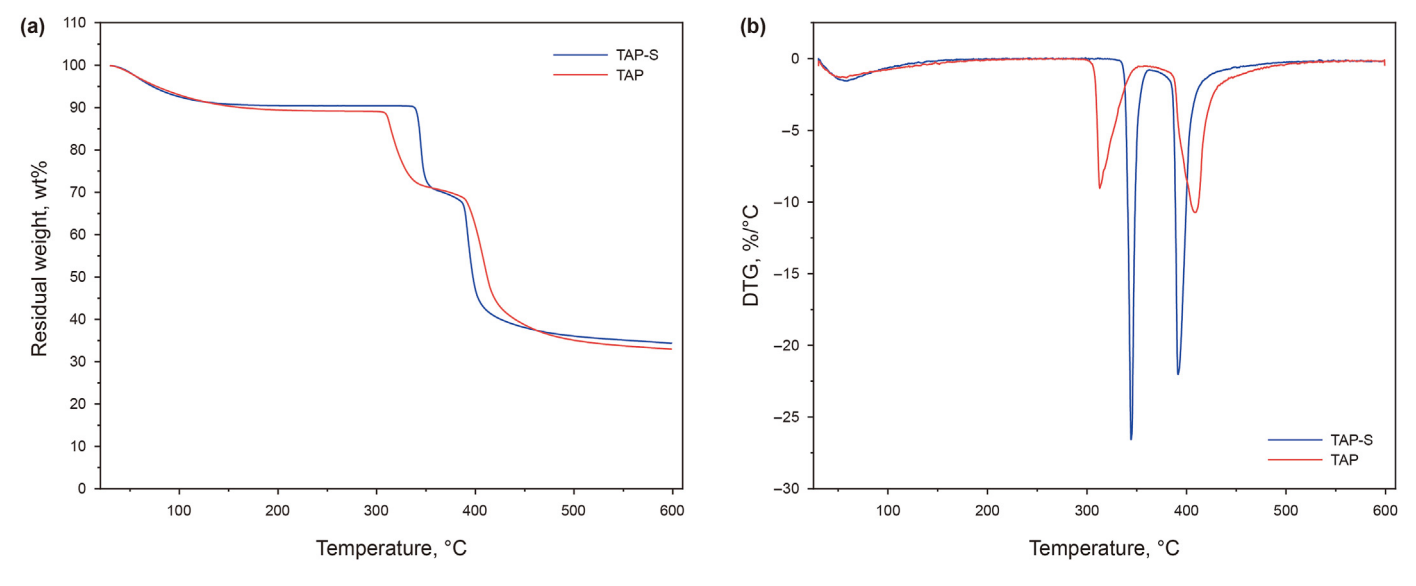


Fig. 7. Thermal analysis of polymeric materials: (a) TGA and (b) DTG.

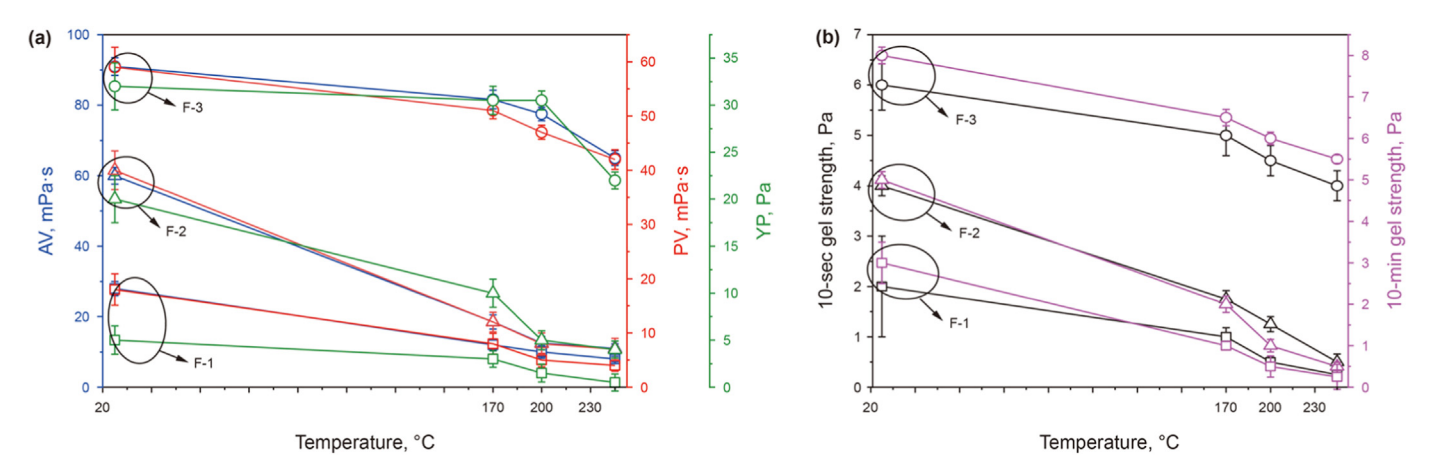


Fig. 8. Rheological properties of drilling fluids at different temperatures (☐ for F-1, △ for F-2, ⊘ for F-3); Note: (a) AV, PV and YP, and (b) 10-sec gel strength and 10-min gel strength.

YP). As indicated in Fig. 8(a), the AV and PV of the TAP-S fluid sample could maintain a nearly 5.6-fold property control compared to F-2 under the same conditions, which revealed that TAP-S was more resilient. This potent viscosifying stability emanating from TAP-S could be attributed to its molecular structure embedded with B-SiNP which contributed not only to reinforcing the thermal conductivity of the viscosity precursor but also reducing the molecular chain motion, and ultimately improving the continuous network in the fluid system. This was particularly beneficial in promoting better particle dispersion and minimizing the flocculation tendency, and eventually maintaining an excellent sweep efficiency under high temperatures (Xie et al., 2023). Similar to the preceding scenario, F-3 could control roughly 6.1-fold of YP compared to F-2, obviously related to the integration of B-SiNP into the molecular skeleton of TAP, resulting in extending the temperature stability of the viscosity precursor, and eventually enhancing the ability of the drilling fluid to carry drill cuttings out of the hole. The improved heat resistance characteristic of TAP-S, contributed to the high flat gel strength trends as shown in Fig. 8(b). This is particularly interesting as it is beneficial for spontaneous gel formation characteristics with high Gel-10s and Gel-10min at 200 °C.

Albeit the rheological properties of the drilling fluid reduced as the temperature extended to 230 °C. The decline was however, minimal under the experimental conditions. The favorable rheology exhibited by F-3 was ascribed to the superior heat resistance characteristic of TAP-S (as previously discussed under TGA analysis). TAP-S admirably improved the rheological properties of LSDFs ascribed to the integration of VB-SiNP into the host TAP, which led to the formation of a solid mixed nanosilica-TAP spatial network structure (which was further explored in the DLS and ESEM experiments).

3.4.2. Filtration loss properties

Drilling fluids with minimal filtration losses under severe conditions is always desirable to avoid several detriments ranging from reduced rock permeability to formation instability (Ezzat et al., 2008; Ibrahim et al., 2017; Shu and Yan, 2008). The filtration properties of TAP-S blended fluids were determined by collecting both the API and HTHP filtration losses volumes and the results were compared with other drilling fluids under identical conditions as indicated in Fig. 9. Contrary to F-1, the filtration loss rate of copolymer fortified fluids declined over time BHR, which was

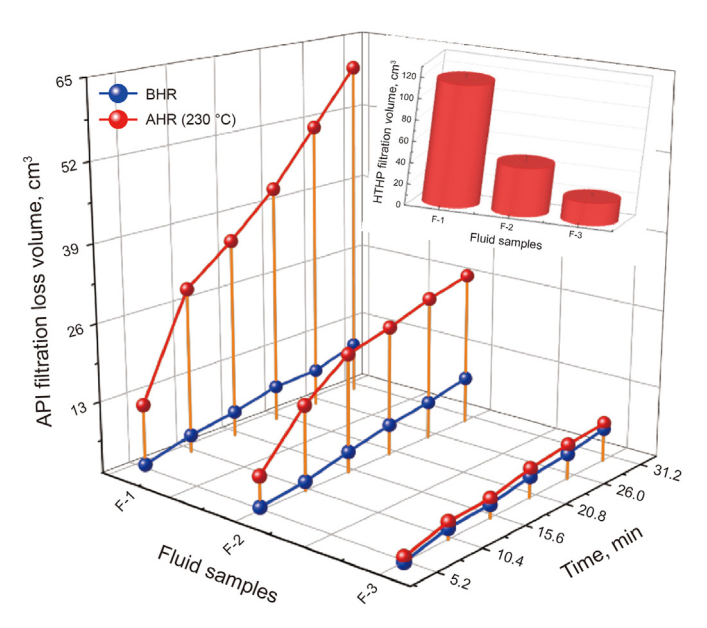


Fig. 9. API filtration properties of drilling fluids at different temperatures (Note: the HTHP filtration indicated in the inset figure).

reflected in the slope of their corresponding experimental curves. The exposure to high temperatures (ca. 230 °C) compromised the filtration properties of the fluid samples and F-1 exhibited the worst filtration controlling capability as it produced the highest filtration loss volume of approximately 60 mL/30 min AHR (ca. 230 °C), followed by F-2 (45 mL) and F-3, which could achieve a 4fold control over F-1 under the same conditions. This trend was also observed under HTHP conditions where the F_{HTHP} declined in the following order: F-1>F-2>F-3 as depicted in the inset figure. From the preceding findings, it can be interpreted that the filtrate loss control properties were not only connected to the thermal stability of the precursor viscosity but also to isolated ionic segments of the host TAP, which interacted with bentonite clay in the fluid system for preventing the flocculation phenomenon beneficial to induce the formation of less permeable filter cake, impeding water intrusion into the formations. Thereby forming a tighter packing structure that can effectively block the voids between the micron-sized particles. This effectively mitigated water ingress into the permeable formations and ultimately diminished the filtrate loss volume (Oseh et al., 2019; Sadeghalvaad and Sabbaghi, 2015).

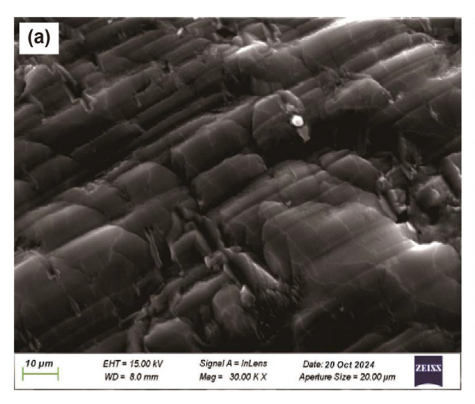
The micro-photographs of filter cake surface topographies of the drilling fluid samples after the heat treatment were further visualized using SEM and represented in Fig. 10. The filter cake surface of the corresponding drilling fluids exhibited distinctive topographies. The high-temperature dehydration contributed to a high degree of flocculation and swelling of bentonite particles with micro-voids on the surface as illustrated in Fig. 10(a), which inevitably favored the intrusion of high-volume filtration loss during the filtration tests. Comparatively, in Fig. 10(b) and (c), it was obvious that the limited temperature conductivity characteristic of TAP contributed to forming a more porous filter cake and less dispersed particles under the studied conditions. Conversely, F-3 produced a well-dispersed bentonite particle decorated with VB-SiNP particle, facilitating the formation of a much more compacted filter cake structure that could clog the water intrusion pathway during the filtration. Therefore, the TAP-S with a special enhanced temperature characteristic could enable better fluid retention of drilling fluid and maintained excellent performance of filter cake to a large extent.

3.4.3. Fluid density

Mud density is a measure of the hydrostatic pressure which tends to control the formation pressure and helps stabilize the wellbore. The fluid samples were weighted to 15 lb/gal and the related data of the fluid densities after the hot-rolling process (ca. 230 °C) were collected to estimate the sagging tendency at inclined (45°) and vertical conditions under static conditions for 24 h according to the density from top and bottom of the fluids using the relationship given in Eq. (4) (Tchameni et al., 2024).

$$Sag\ factor = \frac{bottom\ density}{bottom\ density + top\ density} \tag{4}$$

As noticed in Fig. 11, for both inclined and vertical conditions, F-3 had a sag factor confined between 0.50 and 0.53, which reportedly corresponds to the acceptable range (Tchameni et al., 2024b), whereas the sagging effect is more obvious in F-2 and F-1, indicated by the sag factor over 0.53 mainly attributed to the weakening of intermolecular forces in TAP caused by the thermal deterioration of its molecules under extreme conditions (Hale and Mody, 1993; Liao and Siems, 1990). However, F-3 exhibited a comparatively weaker sagging effect presumably due to the thermal disturbance of the particles (Gupta et al., 2016; Smith et al., 2018). In general, TAP-S demonstrated a certain tendency to reduce the sagging phenomenon in the drilling fluids.



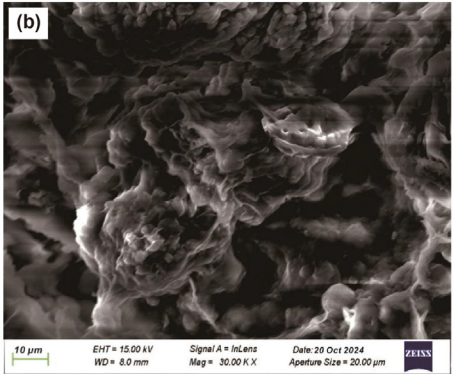




Fig. 10. Filter cake micro-morphology after API filtration tests; (a) F-1; (b) F-2; (c) F-3.

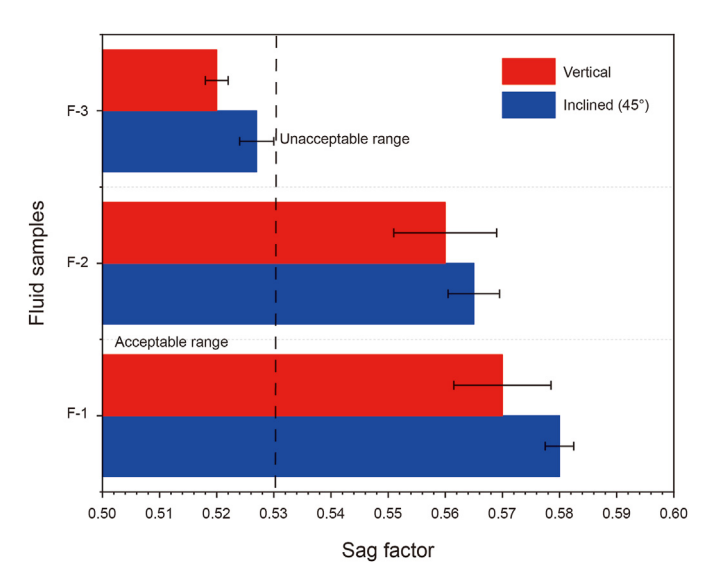


Fig. 11. Density of drilling fluids at different temperatures.

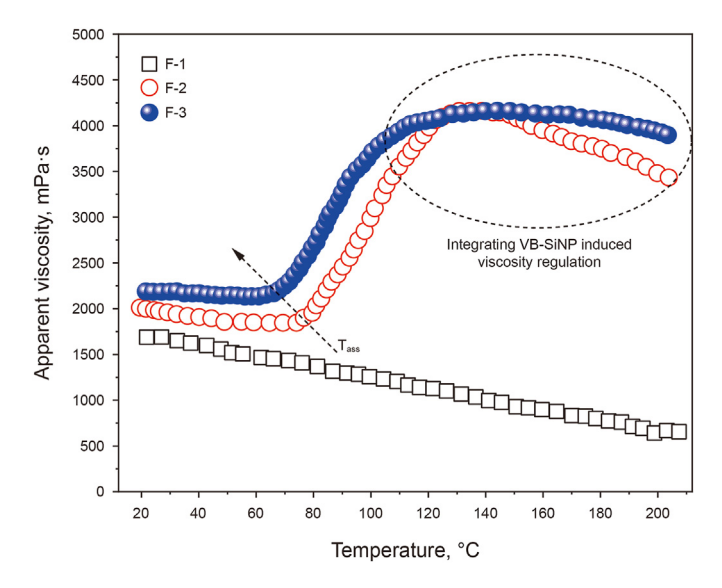


Fig. 12. Thermo-associating behaviour of different viscosity precursors bearing fluids (shear rate = 10 s^{-1} , heating rate = $5 \text{ }^{\circ}\text{C/min}$).

3.5. Thermo-responsive characteristics of drilling fluid under downhole conditions

In this subsection, the thermo-responsive characteristics of F-3 were assessed in terms of rheological properties, steady shear viscosity, and viscoelasticity and compared with those of F-2 and F-1 under the same conditions to understand the contribution of VB-SiNP on flow properties.

3.5.1. Rheological properties of drilling fluids

The viscosities of drilling fluids containing conventional copolymers gradually reduce with increasing temperature according to the Arrhenius-type relationship. This behaviour compromises the lifting capacity of drilled cuttings from the underneath of the wellbore to the surface. However, thermo-associating polymers demonstrate abrupt macroscopic properties with increasing temperatures to offset the above-stated deficiencies to some extent, but environmental concerns were still persistent. To address these

Table 6Values of the activation Gibbs free energies

Fluid samples	Temperature range, ℃	ΔG, kJ/mol	R^2
F-1	20-200	6220	0.939
F-2	20-74	1510	0.935
	130-200	4430	0.965
F-3	20-65	448	0.712
	130-200	1339	0.812

deficiencies, the synergistic effect between biogenic nanomaterials and thermo-associating polymers was explored to improve the thermo-stability of drilling fluids. Given the possibility of physically or chemically combining nanomaterials with polymer to produce nano-hybrid materials, it was worth studying the influence of TAP-S on the rheological properties of LSDFs at high temperatures and comparing the results with that of TAP-bearing fluid under identical conditions.

As the corresponding curves of all the samples shown in Fig. 12 presented regions in which the viscosity gradually diminished upon increasing temperatures ascribed to the in-homogeneities of the phase transition throughout the process, the activation Gibbs energy could be estimated from the well-known Arrhenius relationship given in Eqs. (5) and (6) (Petit et al., 2007a; Portehault et al., 2006).

$$v = v_{\infty} e^{\left(\frac{\Delta G}{RT}\right)} \tag{5}$$

The linearized form is given as:

$$\ln v = \ln v_{\infty} + \frac{\Delta G}{RT} \tag{6}$$

where ν represents the viscosity of the fluid; ΔG denotes the molar activation Gibbs free energy; ν_{∞} represents the pre-exponential term related to the fluid viscosity at "infinite" temperature; R is the universal gas constant; and T is thermodynamic temperature.

As indicated in Fig. 12, the viscosity of fluid F-1 decreased with increasing temperature according to the Arrhenius law, characterized by the highest activation Gibbs free energy (ca. 6220 kJ/mol) as indicated in Table 6, which is expected for fluid incorporated with conventional polymer acting as a viscosity precursor. Conversely, both F-2 and F-3 fluid samples showed thermo-thickening characteristics attributed to the thermo-assembly of LCST precursor of copolymer. The remarkable macroscopic properties were reportedly ascribed to the progressive switch from hydrophilic character to the hydrophobic character of LCST precursors of copolymer additives, which favours hydrophobic association between the thermo-responsive molecular chains (Tchameni et al., 2020). For both experimented fluids, their viscosities reduced with increasing temperature below the threshold (T_{cass}) according to the Arrheniustype relationship. Moreover, the corresponding ΔG of F-3 was much lower than F-2 as listed in Table 6, suggesting that the integration of B-SiNP into the molecular structure of TAP contributed to minimizing a certain energy barrier during the thermo-thinning process. As the temperature increases above the T_{cass} , both F-2 and F-3 exhibited thermo-thickening behaviour with a viscosity reaching the plateau, inferring the formation of a gel-like structure (Portehault et al., 2006). However, the magnitude of the thermothickening effect in the F-3 differed from that in F-2 within the temperature range as shown in the same figure. As it can be deduced, the integration of VB-SiNP not only contributed to diminishing the T_{cass} by 9 °C (ca. F-2 and F-3 were 77 and 66.5 °C, respectively) but also the slope of F-3 rose due to the additional

hydrophobicity arising from the integration nanomaterial. Albeit, both fluids systems reached a plateau at 130 °C, the magnitudes of the thermo-thickening effect of F-2 and F-3 declined by 1.20-fold and 1.05-fold above this region, respectively. In addition, the ΔG of F-3 was still lower than that of F-2, suggesting that the formed gel-like micro-structures in F-3 are more ordered, and it became less plausible for NVCL molecular side chains to leave the formed associated structure (Petit et al., 2007a; Portehault et al., 2006). TAP-S fortified fluid exhibited better macroscopic properties in the whole temperature spectrum emanated from VB-SiNP which induced a solid nano-hybrid micro-cross-linked molecular chain structure, simultaneously resulting in improving heat conductivity characteristic of TAP. Thus, mitigating the excessive copolymer molecular motion, which drives not only the formation of larger hydrophobic domains, but also the instability of the hydrophobic associated structure, and ultimately a weaker spatial network structure at elevated temperatures (Xie and Liu, 2017).

3.5.2. Steady shear viscosity

Typical steady shear viscosities of the fluid samples are shown in Fig. 13. As noticed, F-3 exhibited the highest steady shear viscosity and consistency plots compared to F-2 and F-1 at room temperature and HTHP conditions mainly due to the addition of nanocomposite, which formed solid cross-linked structures with

individual TAP molecular chains in the fluid systems, driving increased steady shear viscosity. Nevertheless, all the fluid systems experienced a decrease in viscosities with no appearance of an obvious plateau with a rising shear rate up to 1200 s^{-1} , indicating an attractive shear thinning (pseudoplastic) behaviour. Comparatively. F-1 was very much sensitive to the increasing temperatures (see Fig. 13 (from (a)–(d)), whereas both F-2 and F-3 systems showed certain thermo-thickening characteristics, which was more obvious in F-3 as a consequence of improving the steady shear viscosity (ca. above 200 °C) as indicated in Fig. 13(d). From the same plots, it can be noticed that F-2 gradually lost its shear thinning behaviour attributable to the deterioration of viscosity precursor TAP. TAP-S referring to TAP with nanomaterials integrated into molecular structures showed enhanced temperature conductivity characteristics resulting to not only in reinforcing the formed continuous network structure in the fluid system, but also mitigate the deleterious of high temperatures on drilling fluids properties, and ultimate prominent improvement of the steady shear viscosity response at high temperatures, especially in the high shear rates region as represented in Fig. 13 ((a) through (d)). Among the studied fluid systems, F-1 defect shear thinning behaviour in a lower shear rate region, that is 0.01-1 s⁻¹ with increasing temperatures, whilst that of F-2 exhibited a sharper drop of this characteristic when exposed to prolonged heat treatment above 200 °C

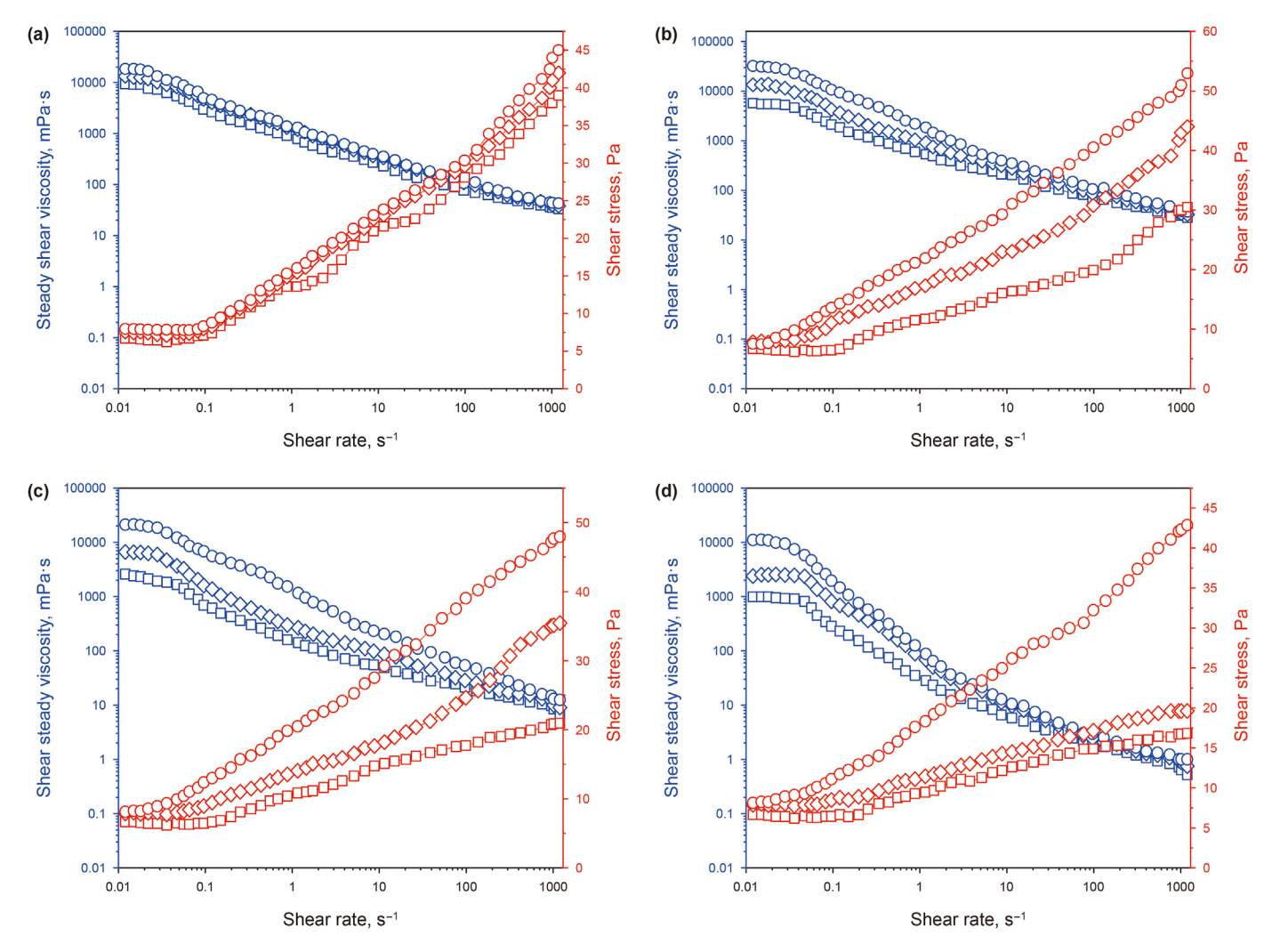


Fig. 13. Steady shear viscosities/shear stress versus shear rate of drilling fluids at different temperatures. Note: (**a**) room temperature; (**b**) 170 °C; (**c**) 200 °C; (**d**) 230 °C; F-1 (□); F-2 (△); F-3 (○).

than F-3, which showed a level of insensitivity upon heating near the zero-shear value, indicating the ability of the nanocomposite to regulate the shear thinning behaviour near the borehole wall. The shear thinning behaviour near the wall aids the control of wall drag that enhances the fluid's lubricity and drives slippage of viscosity precursors in the fluid system at elevated temperatures (Gautam and Guria, 2020). Moreover, a satisfactory thickening effect is believed to increase the viscosity in the annular space. thereby boosting the drilling fluid cleaning efficiency of the wellbore by lifting the cuttings from the drill path while drilling operations (Li et al., 2024; Werner et al., 2017). The low-shear-rate viscosity is essential as it predicts the suspension, mitigates radial slip of drilled cuttings, and minimizes any likelihood for the agglomeration of cuttings beds in the lower part of the wellbore when fluid circulation is ceased in horizontal and extended reach wells (Powell et al., 1991).

In this study, we further attempted to precisely characterize the shear viscosity in this region of shear rate, that is the zero-shear viscosity (μ_0) , the infinite-shear viscosity (μ_∞) , and the flow-behaviour index (n). In total, 3 rheological models were also used to statistically examine the rheological properties of the drilling fluids. Herschel-Bulkley model (Eq. (7)), Cross model (Eq. (8)), and Prandtl-Eyring model (Eq. (9)), which have been used for a quantitative description of drilling fluids rheological properties were applied (Agwu et al., 2021; Tchameni et al., 2021b).

$$\tau = \tau_{01} + k\dot{\gamma}^n \tag{7}$$

$$\tau = \dot{\gamma} \left[\mu_{\infty} + \frac{\mu_0 - \mu_{\infty}}{1 + (\lambda \dot{\gamma})^n} \right] \tag{8}$$

$$\tau = \tau_{o2} + A\sin h^{-1} \left(\frac{\dot{\gamma}}{B}\right) \tag{9}$$

where τ is the shear stress in Pa; τ_{01}, τ_{02} are the yield stress in Pa; $\dot{\gamma}$ is the shear deformation in s⁻¹; k is the consistency index in Pa·sⁿ; μ_{0} is the zero shear viscosity in Pa·s; μ_{∞} is infinite shear viscosity in Pa·s; λ is a natural-time constant; A and B are adjustable constants; n is the flow behaviour index (dimensionless).

From Table 7, which lists all the fitting results, the Cross model consistently produces the maximal correlation coefficient (R^2) reflecting its accuracy in describing the flow behaviour of the studied fluids compared to other rheological models. From the same table, it can be clearly noticed that, the key parameters including μ_0 , μ_∞ , and λ of F-2 significantly varied than those of F-3, indicating the relative stability of the latter when tested in severe geothermal conditions.

3.5.3. Viscoelasticity

3.5.3.1. Dynamic modulus versus angular frequency. Presented in Fig. 14 is the dynamic modulus (G' and G") versus angular frequency (w) for TAP-S or TAP comprising fluids at 25 °C and HTHP conditions (ca. 170, 200, and 230 °C). As can be seen, compared to F-2, F-3 raised the dynamic modulus at 25 °C, which considerably reduced the dependence on angular frequency. This clearly indicates the formation of a hybrid network structure composed of TAP and nanomaterials, which is beneficial for the formation of a stronger mechanical network structure in the fluids. Moreover, the exposure to high temperature also raised the dynamic moduli (~170 °C), indicating the existence of thermo-association behaviour. This contributes to the building of micro-cross-linked network structures driving enhanced viscoelastic character and rheological controlling ability of the fluids under these conditions.

Rheological parameters of drilling fluid samples.

Fluid samples	Herschel-Bulk	Herschel-Bulkley model (Eq. (7))	((2))			Cross model (Eq. (8))	(Eq. (8))				Prandtl-E	yring model (F	(6))	
	Temp., °C	7 ₀₁ , Pa	k, Pa·s ⁿ	и	\mathbb{R}^2	μ _o , Pa·s	μ _∞ , Pa·s	۲	и	R^2	7 ₀₂ , Pa	А	В	\mathbb{R}^2
F-2	25	3.127	1.178	0.567	0.999	110.45	0.0130	15.29	0.450	0.999	2.980	6.586	16. 406	0.995
	170	1.256	0.048	0.756	0.985	67.24	0.0018	20.05	0.7140	0.991	1.391	5.075	11.002	0.935
	200	0.871	0.015	0.871	0.965	23.67	0.0050	27.66	0.748	0.993	0.315	6.285	12.015	0.974
	230	0.376	0.035	0.743	0.920	68.6	0.0011	35.28	0.834	0.995	0.161	2.561	8.031	0.947
F-3	25	4.058	1.480	0.527	0.998	153.21	0.0161	14.43	0.530	0.999	6.186	8.333	26.048	0.660
	170	2.155	1.373	0.569	0.998	139.78	0.0132	17.90	0.471	0.998	4.888	7.797	36.038	0.995
	200	1.821	1.147	0.605	0.991	128.67	0.0115	19.13	0.506	0.989	3.964	9.532	22.032	0.986
	230	1.512	0.860	0.619	0.660	110.04	0.0095	21.30	0.570	0.988	3.056	5.600	20.006	0.987

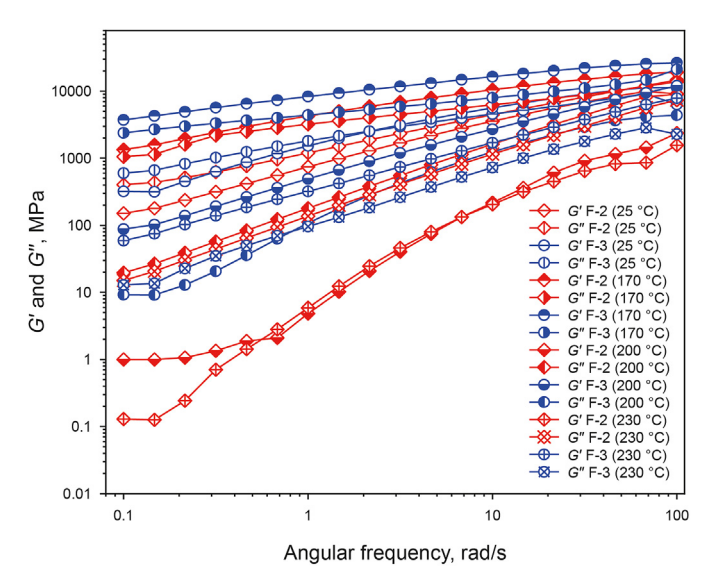


Fig. 14. Dynamic moduli versus angular frequency of fluid samples.

From the same plot (ca. Fig. 14), the corresponding curves of elastic modulus G' exceeded that of viscous modulus G" for both investigated fluids, reflecting the formation of a gel-like structure under these conditions. In general, the dynamic modulus of F-3 was higher than those of F-2 ascribed to the substantial hydrophobicity of the B-SiNP, which contributed to reinforcing the strength of the hydrophobic association to a certain extent aroused from the interaction between LCST precursor. Further heat treatment up to 230 °C prominently reduced the dynamic modulus, characterized by the loss of the elastic property as the corresponding curves of the loss modulus (G'') overtook those of the storage modulus (G') in F-2 under the studied conditions. Comparatively, albeit the F-3 gradually reduced the dynamic modulus when tested under the same conditions, the elastic property was still dominant in the fluid. These findings infer that the integration of VB-SiNP could enhance the formation of continuous micro-structure in the fluid system. This type of behaviour was indicative of the formation of a complex network structure mainly originating from stronger interaction between the LCST precursor in TAP and VB-SiNP-3, which exhibited better dispersion in aqueous medium (which was indicated in TEM analysis). Therefore, the relatively stable formed gel-like structure might improve the fluid rheological flow, which is beneficial to promote better-drilled cuttings lifting capacity with a significant reduction in annular friction pressure drop at high temperatures.

3.5.3.2. Normal stress. The quantification of elastic energies generated by TAP-S and TAP was studied by comparing the normal stress-shear rate profile of both fluid samples as represented in Fig. 15. It is noticed that the normal stress responses of F-3 were considerably higher compared to those of F-2 confirming that the former is dominated with stronger elastic structures throughout the studied temperatures. In this study, we further attempted to correlate the elastic character of the formed network structure to the relaxation time (θ) using the mathematical expression given in Eq. (10).

$$\theta = \frac{N_1}{2\eta\dot{\gamma}} \left(\frac{1}{\dot{\gamma}}\right) \tag{10}$$

where N_1 is the first normal stress difference in Pa, η is the shear viscosity in mPa·s, and $\dot{\gamma}$ is the shear rate in s⁻¹.

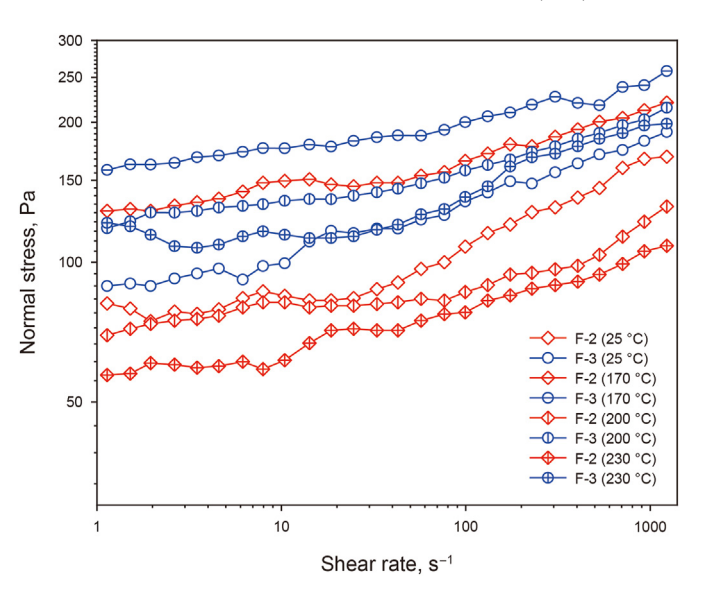


Fig. 15. Normal stress versus shear rate of fluid samples.

3.5.3.3. Relaxation time. The estimated relaxation time versus the shear rate of both fluid samples were compared in Fig. 16. It was noted that the value of θ diminished with increasing $\dot{\gamma}$ throughout the studied ramp of temperature. Comparatively, the θ of F-3 demonstrated considerably the least dependence on hot rolling treatment. Consequently, we could expect a marginal difference between the time required for this fluid to relax at high temperatures and room temperature after being stressed during fluid circulation. This is particularly advantageous in the formation of an instantaneous gel characteristic with a flat rheological profile at high temperatures (see Fig. 8(a) and (b)).

3.6. Mechanism of rheology regulation

In this subsection, the integration of VB-SiNP into the molecular structure of TAP with respect to the thermo-stability mechanism in aqueous medium was first elucidated, followed by the clarification in bentonite fluid.

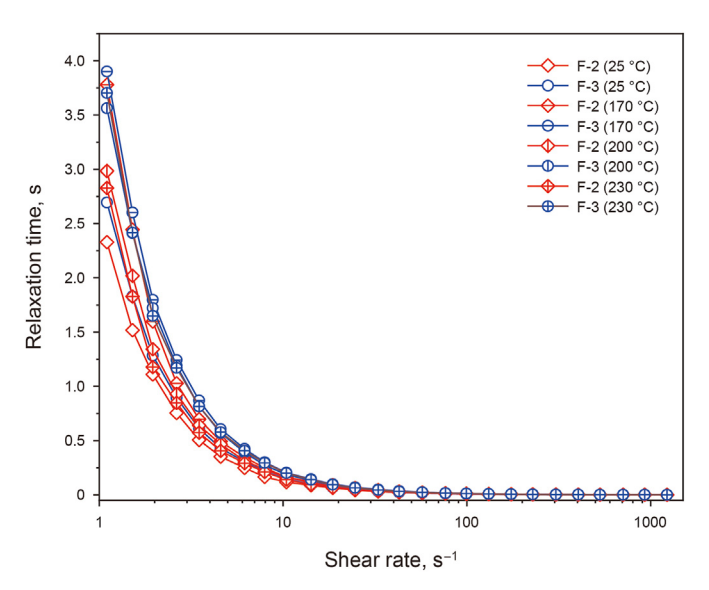


Fig. 16. Relation time versus shear rate of fluid samples.

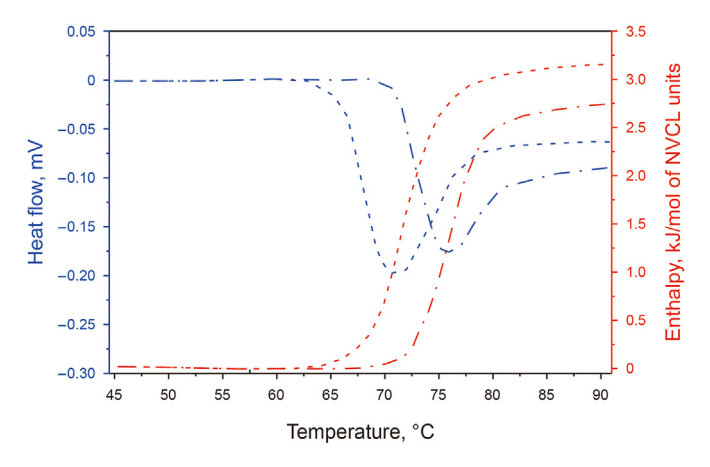


Fig. 17. DSC analysis of TAP and TAP-S aqueous solutions ($C_p = 1.5$ wt%, heating rate = 2 °C/min; dash-dot line for TAP and dash line for TAP-S).

3.6.1. Thermo-stability mechanism in aqueous medium

3.6.1.1. DSC analysis. The thermo-associative process of LCST-based copolymers is apparently endothermic where the transition enthalpy could be used to study the dynamic behaviour of thermo-responsive chains. Therefore, the DSC analysis was used to hypothesize the thermo-associative process by tracking the impact of VB-SiNP on the phase segregation and transition heat of TAP solution.

As indicated in Fig. 17, both the transition enthalpy and phase segregation temperature (LCST) of the nanohybrid materials solutions were compared with that of the TAP solution under similar conditions. Compared with TAP ($\Delta H = 2.76$ kJ/mol of NVCL), TAP-S produced a higher transition enthalpy of approximately, 3.16 kl/mol of NVCL. The LCST of TAP-S and TAP solutions were \cong 62.5 °C and 72 °C, respectively. The preceding values of LCST were consistently lower than that of T_{cass} obtained by rheological analysis in Fig. 11 probably due to a certain steric hindrance aroused by the drilling fluid additives (Tchameni et al., 2021b). As VB-SiNP nanomaterials with a certain level of hydrophobicity were covalently bound to TAP, the nano-hybrid not only demonstrated a substantial hydrophobicity contributed to reinforcing the hydrophobic association phenomenon. Consequently, the LCST was observed at a relatively low temperature. In this regard, a lower temperature is required to drive dehydration of the residual fraction of LCST in nano-hybrid structures than TAP. Thus, lower energy was expected to disintegrate the residual hydrogen bonds formed between the LCST chains and surrounding water molecules at elevated temperatures since the transition enthalpy is largely connected to this energy.

3.6.1.2. DLS analysis. From the DLS results indicated in Fig. 18, the HD of TAP-S was lower than TAP, which agreed with the profile of the viscosity enhancement of the drilling fluid as earlier observed. The experimental data revealed that the temperature at which an obvious reduction in HD occurred was not identical to the inflection point temperature of the fluid rheological curves shown in Fig. 8. The dissimilarity between these two temperatures plausibly originated from the addition of oxygen scavengers (Na₂SO₃) to drilling fluids, which was frequently introduced in the polymer fluids to minimize the thermo-oxidative deterioration of polymer molecule, thereby boosting the thermo-stability of fluids to greater extent. However, comparing Figs. 8 and 9, it was evidently noticed that the role of Na₂SO₃ was restricted. As indicated in Fig. 18, it was noted that AMS-CGBA preserved more than half (~59.34%) of its initial HD up to the oven-treatment temperature of 230 °C, which was superior to that of TAP (~29.29%) when tested under the same

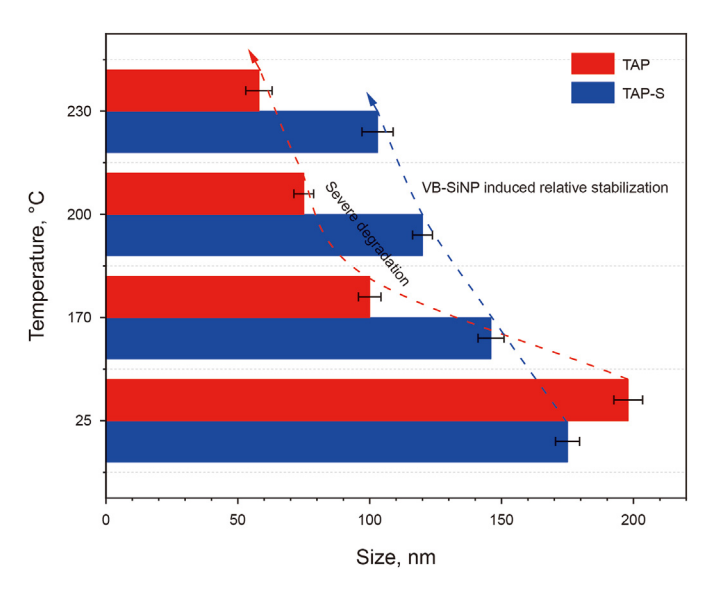


Fig. 18. Hydrodynamic size of polymer and nano-hybrid materials solutions versus aging temperatures.

conditions. The preceding results indicate that the covalently bounded VB-SiNP to TAP was predisposed to retard the cleavage of the polymer molecular backbone. Thereby, strengthening the heat transfer characteristic of TAP.

3.6.1.3. Micro-morphology analysis. The ESEM micro-photographs of TAP and TAP-S solutions are depicted in Fig. 19. Compared to the corresponding micro-photographs of TAP, that of TAP-S clearly ascertained the presence of continuously aggregated morphologies with several interesting features. The 3D-network structures decorated with nanomaterials could be observed in the solution. These formed mixed B-SiNP-TAP network structures which prompted an enhanced heat transfer characteristic of the 3Dnetwork structures. This phenomenon was beneficial for preserving the thickening properties at high temperatures. Compared to Fig. 19(a) and (b) demonstrated obviously integrated 3D-network structure, which promoted attractive thickening properties and formed a solid nano-hybrid network structure. This presumably meant that TAP was chemically cross-linked by VB-SiNP via strong covalent bounding. The phenomenon effectively retards the reaction on the amide group between H⁺ and OH⁻ at elevated temperatures, reduced the heat sensitivity of key functional groups, and ultimately conferred potent protection in the host TAP molecular structure (Cao et al., 2018a). Thus, improving the thermal stability, and eventually the preservation of certain thickening properties in aqueous solutions. The preceding results were consistent with those obtained in rheological analysis (As seen in Fig. 8).

3.6.2. Thermal stability in bentonite fluids

3.6.2.1. EPM analysis. The colloidal dispersion stability was also studied by tracking the EPM of Mt particles in the presence of polymeric materials. The results were compared with the free-polymeric materials system in the temperature range of 25–230 °C as indicated in Fig. 20. It was clearly noticed that the addition of polymeric materials into Mt dispersion increased the EPM, which was expected as the edge charges of Mt platelets were screened with anionic groups in the polymeric molecular structure, leading to the electrostatic repulsion between the colloidal particles, and ultimately a more dispersed state (Tchameni et al., 2024b). The exposure to heat treatment up to 230 °C had a detrimental

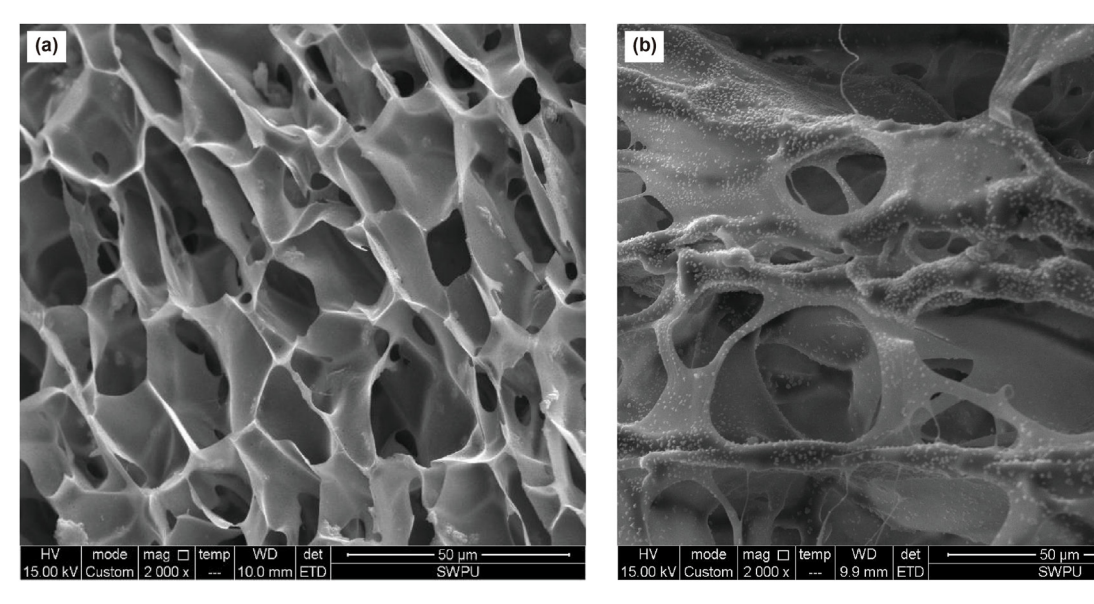


Fig. 19. Micro-morphology of polymeric materials in distilled water. (a) TAP and (b) TAP-S.

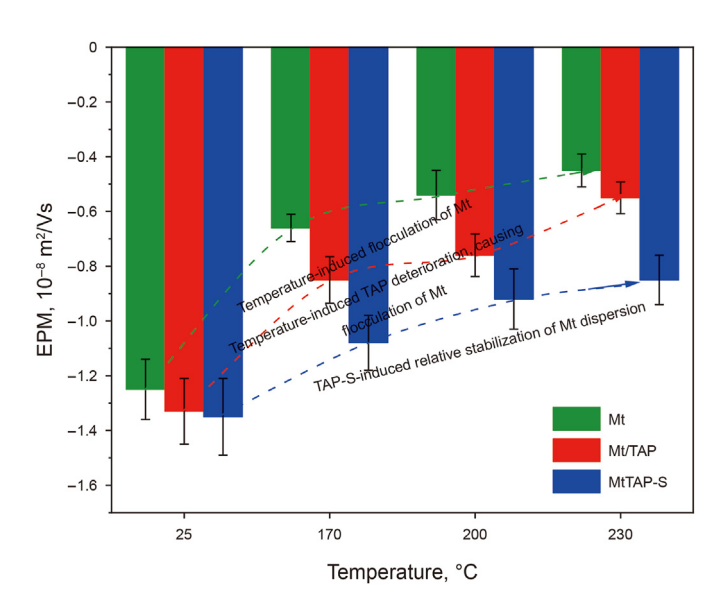


Fig. 20. EPM of polymeric materials in bentonite fluids.

impact on Mt dispersion as the EPM reduced by more than half (ca from -1.25 to $-0.45\times 10^{-8}\,\text{m}^2/\text{V}_\text{s}$) due to significant suppression of the thickness of the electric double layer causing particle flocculation and settling. The Mt/TAP system was not exempted from this phenomenon as the corresponding EPM shares the same pattern with those of Mt because of the deterioration of TAP molecular structures (which was investigated in the previous DLS analysis). Albeit the Mt/TAP-S system also showed a certain reduction in EPM, it consistently maintained the highest values at each studied temperature, reflecting its better dispersal stability due to the solid-hybrid network structure, enabling the interactions between the ionic groups along the molecular chains and Mt platelets, which conferred potent protection on Mt platelets as a result of mitigating fluid ingress and maintaining rheological flow stability.

3.6.2.2. Particle size distribution analysis. The results of particle size distribution measurements at 25 and 230 °C displayed in Fig. 21(a) and (b) revealed that the addition of polymeric materials into

bentonite reduced the mean particle size compared to the bentonite system alone at 25 °C with a much greater effect in Bent/TAP-S due to the smaller particle size of TAP-S relative to TAP (which was examined in the previous DLS). In both scenarios, it could be speculated that the polymeric materials could bind to the surface of bentonite particles without altering the particle sizes. After the heat treatment at 230 °C for 16 h, a noticeable increase in the mean particle size was observed owing to the deterioration of TAP. Under this circumstance, the high-temperature dehydration effect simultaneously promoted particle flocculation, which was also connected to the increasing tendency in particle size in the bentonite system alone. In contrast, the bent/TAP-S showed relative stability of the capability of TAP-S to effectively disperse bentonite particles, thus mitigating the flocculation for effective rheological flow at high temperatures.

3.7. Rheological stabilization mechanism

Based on the preceding findings, the characteristic of thermoassociating nano-hybrid structures is shown in Fig. 22. Clay particles are composed of platelets with negatively charged sites, edges, and its electrical potential depending on the pH of the fluids. The edges of bentonite platelets become positively charged (Al-OH²⁺), while it becomes electrically neutral (Al-OH) at pH = 7 and change to Al -0^- at a pH > 7 (Tchameni et al., 2024a). On the one hand, it can be hypothesized that, as B-SiNP nanomaterial was chemically bounded to TAP via strong covalent bonding creating a solid nanohybrid system (which was investigated early in DLS analysis) with not only favorable temperature stability ascribed to a potent heat transfer characteristic, but also thickening characteristics aroused from both thermo-association processes by the hydrophobic interaction (which was also studied in the DSC analysis). This permitted the formation of a mixed complex continuous network structure B-SiNP-TAP network structures, which was particularly advantageous to enhancing the thermal conductivity leading to mitigate the deleterious effect of prolonged heat treatments in the fluid. On the other hand, as sulfonyl functional groups in the AMPS subunits of nano-hybrid material could specifically interact with bentonite platelets via electrostatic attractions (Shaikh et al., 2018), TAP-S could wrap onto the clay particles conferring a certain protection against the thermal deterioration, and simultaneously

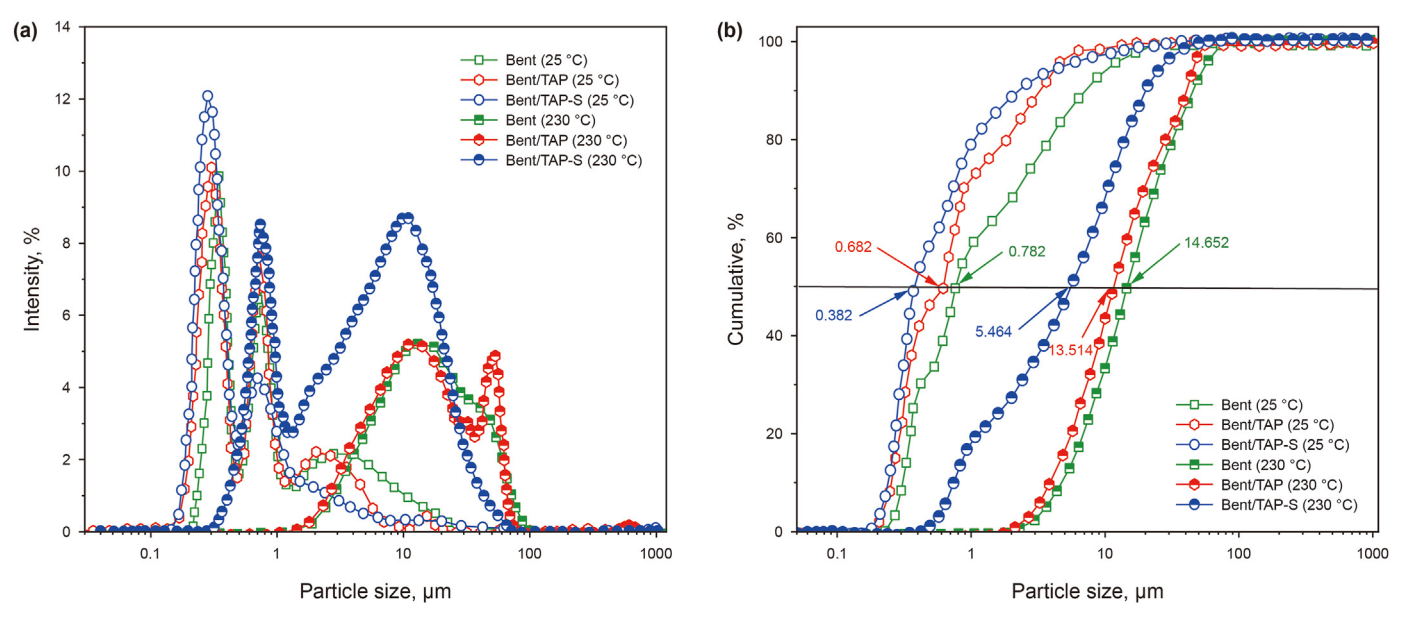


Fig. 21. (a) Intensity; (b) cumulative of polymeric materials in bentonite fluids.

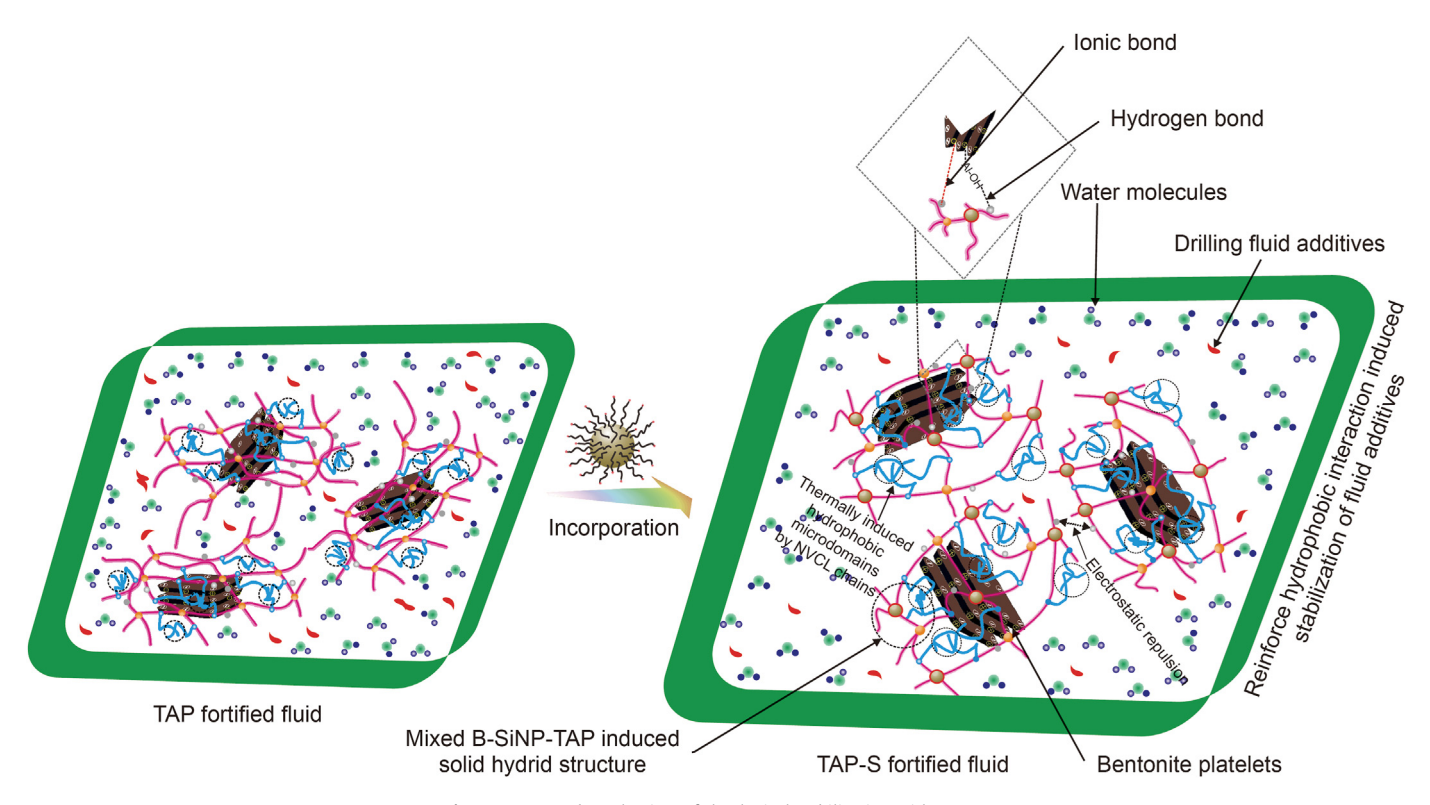


Fig. 22. Proposed mechanism of rheological stabilization with TAP-S.

enhancing the hydration shell of clay particles, which partially contributed to fluid viscosification for better suspension capacity of the fluid additives, for simultaneously attractive rheological flow, filtration loss control, and optimal performance at high temperatures.

TAP-S considerably improved the ability of LSDFs to withstand the gradual increase rise in temperature while flowing in the wellbore and reduce heat as the fluids return to the surface, and it ultimately expected to show great efficiency in regulating the rheology, and filtration loss of the fluid while also mitigating the negative impact to the environment during deep-well drilling operations.

3.8. Economic perspective of biogenic-SiNP over commercial synthetic SiNP

At present, albeit production is at the laboratory stage, biogenic-SiNP showed economic feasibility in many aspects. Firstly, their sources especially RH is inexpensive and widely available as well as an environmentally friendly waste used for the preparation of biogenic-SiNP under relatively lower temperatures (ca. 700 °C) than the commercial synthetic SiNP which are produced from expensive precursors (ca. sodium silica and tetra ethyl silica) at 1300 °C and required toxic chemical, and stringent reaction conditions for a prolonged period. Therefore, the energy and cost implications related to the extraction of commercial synthetic SiNP are quite high compared to more cost-effective approach for biogenic-SiNP (Mor et al., 2017). In this regard, the cost of raw materials and energy consumption for the production of SiNP from RH having a particle size ranging between 10 and 20 nm and purity> 98% reportedly had a net profit of 65.75 \$ compared to the commercial ones (Mor et al., 2017). Secondly, a large quantity of Greenhouse gas (GHG) is emitted (ca. CO₂) during the preparation process of the commercial synthetic SiNP, causing global warming. Contrarily, the net emission from the calcination of RHs is considered zero as per IPCC guidelines (Mor et al., 2017). Thus, the extraction of biogenic-SiNP could significantly minimize GHG emissions and ultimately help attain the Paris Agreement's goals (International Energy Agency, 2020). Based on the above cogent reasons, the biogenic-SiNP is well positioned as a versatile and suitable NPs for a wide spectrum of industrial applications.

4. Conclusions

This work discloses the feasibility of using biogenic nanosilica to strengthen the molecular structure of thermo-associating polymer as additives in LSDFs at high temperatures. A thermo-associating copolymer nano-hybrid material TAP-S was successfully synthesized by in-situ polymerization, and the molecular structure was characterized by FT-IR, ¹H-NMR, elemental analysis, TGA, and zeta potential measurement. F-3 demonstrated higher steady shear viscosity throughout the studied temperature range than its counterpart's F-2. Moreover, F-3 practically maintained 80% of its initial rheological properties with lower filtration loss volume and was prone to less sagging phenomenon compared to F-2 and F-1 after the hot rolling process at 230 °C. Based on the rheological properties, the thermo-thickening effect of F-3 became prominent compared to F-2 in the temperature range of 70-210 °C because of the strong synergistic effect between the thermo-associating polymer and hydrophobic B-SiNP, which promoted a certain thermal conductivity characteristic, binding onto the surface of bentonite particles to mitigate the flocculation tendency at high temperatures. This was responsible for mitigating the temperature dependence of the η , N_1 , and θ , which is particularly beneficial for the formation of instantaneous gel while drilling operations. The thermo-associating amended biogenic nanosilica could serve as a potential candidate for regulating the rheological properties of high-temperature low-solid drilling fluid while mitigating the negative impact on the flora.

CRediT authorship contribution statement

Alain Pierre Tchameni: Writing — original draft, Methodology, Investigation, Funding acquisition, Formal analysis, Conceptualization. Robert Dery Nagre: Writing — review & editing, Validation, Data curation. Shu-Ming Yin: Writing — review & editing, Validation. Li-Qiang Wang: Writing — review & editing, Validation. Supervision. Xiu-Ying Wang: Writing — review & editing, Visualization, Validation. Si-Yuan Zhou: Validation, Writing — review & editing, Validation. Xu-Dong Wang: Writing — review & editing, Validation, Validation, Data curation.

Declaration of competing interest

The authors declare that they have no known competing financial interests or personal relationships that could have appeared to influence the work reported in this paper.

Acknowledgments

This work was financially supported by the National Natural Science Foundation for International Young Scientists of China (Grant No. 52150410427), and funding of Scientific Research Start-up Project for High-Level Talents of Shandong Institute of Petroleum and Chemical Technology (Grant No. DJB2023020 and Grant No. 2023SS019).

Nomenclature

A, B	Adjustable constants
AIBI	2,2'-azobis[2-(2-imidazolin-2-yl)propane]
	dihydrochloride
AMPS	2-acrylamido-2-methylpropane sulfonic acid
API	American Institute of Petroleum
AV	Apparent viscosity
B-SiNP	Biogenic nanosilica
B-SiNP-TA	P, TAP-S: Biogenic nanosilica-hybrid material
$CaCO_3$	Calcium carbonate
DLS	Dynamic light scattering
DSC	Differential scanning calorimetry
EPM	Electrophoretic mobility
ESEM	Environmental scanning electron microscopic
L+OII	Tth an al

EtOH Ethanol
F-1 Base fluid
F-2 Base fluid + TAP
F-3 Base fluid + TAP-S
G' Storage modulus
G'' Loss modulus

 ΔG Molar activation Gibbs free energy

H Cumulated enthalpy
HD Hydrodynamic diameter

HTHP High temperature high pressure

k Consistency index

LCST Lower critical solution temperature

LSDF Low solid drilling fluid λ : Natural-time constant MBA N,N'-methylenebisacrylamide Mt Sodium montmorillonites $\mu_{\rm o}$: Zero shear viscosity μ_{∞} : Infinite shear viscosity

 μ_{∞} : Infinite shear viscosity n Flow behaviour index η Shear steady viscosity N_1 : Normal stress

NVCL: N-vinylcaprolactam
NaOH Sodium hydroxide
Na₂CO₃ Sodium carbonate
Na₂SO₃ Sodium sulfite
θ Relaxation time
PV Plastic viscosity
R Universal gas constant

RHs Rice husks

ROP Rate of penetration
SLSDF Smart low-solid drilling fluid

SEM Scanning electron microscopy
VTES Vinyl triethoxysilane
TAP Thermo-associating polymer

v: Viscosity of the fluid

 v_{∞} : Pre-exponential term related to the fluid viscosity at

"infinite" temperature

VB-SiNPs Vinyl-terminated biogenic nanosilica

WBDFs Water-based drilling fluids

T Temperature τ : Shear stress τ_{o1}, τ_{o2} : Yield stress

 $T_{\rm cass}$ Threshold temperature

TEA Trimethylamine

TEM Transmission electron microscopy
TGA Thermal gravimetry analysis

TSI Turbiscan stability index

YP Yield point

 $\dot{\gamma}$: Shear deformation

References

- Agwu, O.E., Akpabio, J.U., Ekpenyong, M.E., Inyang, U.G., Asuquo, D.E., Eyoh, I.J., Adeoye, O.S., 2021. A critical review of drilling mud rheological models. J. Pet. Sci. Eng. 203, 108659. https://doi.org/10.1016/j.petrol.2021.108659.
- Al-Oweini, R., El-Rassy, H., 2009. Synthesis and characterization by FTIR spectroscopy of silica aerogels prepared using several Si(OR)₄ and R"Si(OR')₃ precursors. J. Mol. Struct. 919 (1–3), 140–145. https://doi.org/10.1016/j.molstruc.2008.08.025.
- API Recommended Practice, 2009. API Recommended Practice for Field Testing Water-Based Drilling Fluids, fourth ed. ANSI/API Recommended Practice. 13B-1. https://tajhizkala.ir/doc/API/API_RP_13B_1_2014_,_Recommended.pdf.
- Cao, J., Song, T., Wang, X., Zhu, Y., Wang, S., Zhao, M., Miao, Y., Zhang, J., 2019. Studies on the rheological properties of amphiphilic nanosilica and a partially hydrolyzed polyacrylamide hybrid for enhanced oil recovery. Chem. Eng. Sci. 206, 146–155. https://doi.org/10.1016/j.ces.2019.05.034.
- Cao, J., Song, T., Zhu, Y., Wang, S., Wang, X., Lv, F., Jiang, L., Sun, M., 2018a. Application of amino-functionalized nanosilica in improving the thermal stability of acrylamide-based polymer for enhanced oil recovery. Energy Fuels 32 (1), 246–254. https://doi.org/10.1021/acs.energyfuels.7b03053.
- Cao, J., Song, T., Zhu, Y., Wang, X., Wang, S., Yu, Ba, Y., Zhang, J., 2018b. Aqueous hybrids of amino-functionalized nanosilica and acrylamide-based polymer for enhanced oil recovery. RSC Adv. Royal Society of Chemistry 8 (66), 38056–38064. https://doi.org/10.1039/C8RA07076H.
- Chen, Q., Wang, Y., Lu, Z., Feng, Y., 2013. Thermoviscosifying polymer used for enhanced oil recovery: rheological behaviors and core flooding test. Polym. Bull. 70 (2), 391–401. https://doi.org/10.1007/s00289-012-0798-7.
- da Luz, R.C.S., Paixão, M.V.G., de, C., Balaban, R., 2019. Nanosilica-chitosan hybrid materials: preparation, characterization and application in aqueous drilling fluids. J. Mol. Lig. 279, 279—288. https://doi.org/10.1016/j.mollig.2019.01.131.
- fluids. J. Mol. Liq. 279, 279–288. https://doi.org/10.1016/j.molliq.2019.01.131. Djouonkep, L.D.W., Xie, B., Tao, H., Chen, J., Zhua, L., Selabi, N.B.S., Zhao, L., 2024. Enhanced amphoteric polymer filtration reducer with vinyl-functionalized nanosilica for high-salt and ultra-high temperature water-based drilling environments. Geoenergy Sci. Eng. 236, 212743. https://doi.org/10.1016/j.geoen. 2024.212743.
- Durand, A., Hourdet, D., 1999. Synthesis and thermoassociative properties in aqueous solution of graft copolymers containing poly(N-isopropylacrylamide) side chains. Polymer 40 (17), 4941–4951. https://doi.org/10.1016/S0032-3861(98)00698-3.
- Ezzat, A.M., Gamal, M., D'Angelo, S., 2008. High-density brine-based drill-in fluid improved reservoir producibility in gas field offshore Egypt. SPE - North Africa Technical Conference and Exhibition, Marrakech, Morocco, pp. 497–507. https://doi.org/10.2118/112950-MS.
- Gautam, S., Guria, C., 2020. Optimal synthesis, characterization, and performance evaluation of high-pressure high-temperature polymer-based drilling fluid: the effect of viscoelasticity on cutting transport, filtration loss, and lubricity. SPE J. 25 (3), 1333–1350. https://doi.org/10.2118/200487-PA.
- Guo, H., Brûlet, A., Rajamohanan, P.R., Marcellan, A., Sanson, N., Hourdet, D., 2015. Influence of topology of LCST-based graft copolymers on responsive assembling in aqueous media. Polymer 60, 164–175. https://doi.org/10.1016/j.polymer.2015.01.038.
- Guo, Y., Wang, M., Zhang, H., Liu, G., Zhang, L., Qu, X., 2008. The surface modification of nanosilica, preparation of nanosilica/acrylic core-shell composite latex, and its application in toughening PVC matrix. J. Appl. Polym. Sci. 107 (4), 2671–2680. https://doi.org/10.1002/app.27310.
- Gupta, V., Magotra, U.S., Sharma, A.K., Sharma, M., 2016. A study of concentration and temperature dependent effect on speed of sound and acoustical parameters in zinc oxide nanofluid. Science International 4 (2), 39–50. https://scialert.net/ abstract/?doi=sciintl.2016.39.50.
- Hale, A.H., Mody, F.K., 1993. Partially hydrolyzed polyacrylamide (PHPA) mud systems for Gulf of Mexico deepwater prospects. SPE International Symposium on Oilfield Chemistry, New Orleans, Louisiana, pp. 301–316. https://doi.org/10.2118/25180-MS.

- Harish, R., Sivakumar, R., 2021. Turbulent thermal convection of nanofluids in cubical enclosure using two-phase mixture model. Int. J. Mech. Sci. 190, 106033. https://doi.org/10.1016/j.ijmecsci.2020.106033.
- Hayat, T., Khan, M.I., Waqas, M., Alsaedi, A., 2017. Effectiveness of magnetic nano-particles in radiative flow of Eyring-Powell fluid. J. Mol. Liq. 231, 126–133. https://doi.org/10.1016/j.molliq.2017.01.076.
- Hourdet, D., L'Alloret, F., Audebert, R., 1994. Reversible thermothickening of aqueous polymer solutions. Polymer 35 (12), 2624–2630. https://doi.org/10.1016/0032-3861(94)90390-5.
- Ibrahim, D.S., Sami, N.A., Balasubramanian, N., 2017. Effect of barite and gas oil drilling fluid additives on the reservoir rock characteristics. J. Pet. Explor. Prod. Technol. 7 (1), 281–292. https://doi.org/10.1007/s13202-016-0258-2.
- International Energy Agency, 2020. The oil and gas industry in energy transitions. https://www.iea.org/reports/the-oil-and-gas-industry-in-energy-transitions.
- Jain, R., Mahto, V., 2017. Formulation of a water-based drilling fluid system with synthesized graft copolymer for troublesome shale formations. J. Nat. Gas Sci. Eng. 38, 171–181. https://doi.org/10.1016/j.jngse.2016.12.018.
- Keshavarz Moraveji, M., Ghaffarkhah, A., Agin, F., Talebkeikhah, M., Jahanshahi, A., Kalantar, A., Saman Fazel Amirhosseini, S.F., Karimifard, M., Mortazavipour, S.I., Sehat, A.A., Arjmand, M., 2020. Application of amorphous silica nanoparticles in improving the rheological properties, filtration and shale stability of glycolbased drilling fluids. Int. Commun. Heat Mass Tran. 115, 104625. https://doi.org/10.1016/j.icheatmasstransfer.2020.104625.
- Li, J., Ji, Y.X., Ni, X.X., Lv, K., Huang, X., Sun, J., 2024. A micro-crosslinked amphoteric hydrophobic association copolymer as high temperature- and salt-resistance fluid loss reducer for water-based drilling fluids. Pet. Sci. 21 (3), 1980–1991. https://doi.org/10.1016/j.petsci.2024.01.021.
- Li, M., Ren, S., Zhang, X., Dong, L., Lei, T., Lee, S., 2018. Surface-chemistry-tuned cellulose nanocrystals in a bentonite suspension for water-based drilling fluids. ACS Appl. Nano Mater. 1 (12), 7039–7051. https://doi.org/10.1021/acsanm.8b01830.
- Li, M., Wu, Q., Song, K., De Hoop, C.F., Lee, S., Qing, Y., 2016. Cellulose nanocrystals and polyanionic cellulose as additives in bentonite water-based drilling fluids: rheological modeling and filtration mechanisms. Ind. Eng. Chem. Res. 55 (1), 133–143. https://doi.org/10.1021/acs.iecr.5b03510.
- Li, M., Wu, Q., Song, K., Qing, Y., Wu, Y., 2015. Cellulose nanoparticles as modifiers for rheology and fluid loss in bentonite water-based fluids. ACS Appl. Mater. Interfaces 7 (8), 5009–5016. https://doi.org/10.1021/acsami.5b00498.
- Li, X., Xu, Z., Yin, H., Feng, Y., Quan, H., 2017. Comparative studies on enhanced oil recovery: thermoviscosifying polymer versus polyacrylamide. Energy Fuels 31 (3), 2479–2487. https://doi.org/10.1021/acs.energyfuels.6b02653.
- Liao, W., Siems, D.R., 1990. Adsorption characteristics of PHPA on formation solids. IADC/SPE Drilling Conference. Houston, Texas. https://doi.org/10.2118/19945-MS
- Liou, T.H., 2004. Preparation and characterization of nano-structured silica from rice husk. Materials Science and Engineering: A 364 (1–2), 313–323. https://doi.org/10.1016/j.msea.2003.08.045.
- Liu, F., Yao, H., Liu, Q., Wang, X., Dai, X., Zhou, M., Wang, Y., Zhang, C., Wang, D., Deng, Y., 2021. Nano-silica/polymer composite as filtrate reducer in water-based drilling fluids. Colloids and Surface A 627, 127168. https://doi.org/10.1016/ j.colsurfa.2021.127168.
- Mao, H., Qiu, Z., Shen, Z., Huang, W., 2015. Hydrophobic associated polymer based silica nanoparticles composite with core-shell structure as a filtrate reducer for drilling fluid at ultra-high temperature. J. Pet. Sci. Eng. 129, 1–14. https:// doi.org/10.1016/j.petrol.2015.03.003.
- Mao, H., Qiu, Z., Xie, B., Wang, Z., Shen, Z., Hou, W., 2016. Development and application of ultra-high temperature drilling fluids in offshore oilfield around Bohai Sea Bay basin, China. SPE Offshore Technology Conference Asia. Kuala Lumpur, Malaysia. https://doi.org/10.4043/26384-MS.
- Mor, S., Manchanda, C.K., Kansal, S.K., Ravindra, K., 2017. Nanosilica extraction from processed agricultural residue using green technology. J. Clean. Prod. 143, 1284–1290. https://doi.org/10.1016/j.jclepro.2016.11.142.
- Ma, C., Tchameni, A.P., Pan, L., Su, C., Zhou, C., 2020. A thermothickening polymer as a novel flocculant for oily wastewater treatment. Separ. Sci. Technol. 55 (1), 123–134. https://doi.org/10.1080/01496395.2018.1563161.
- Martín-Alfonso, M.J., Pozo, J., Delgado-Sánchez, C., Martínez-Boza, F.J., 2021. Thermal and rheological properties of hydrophobic nanosilica in sunflower oil suspensions at high pressures. Nanomaterials 11 (11), 3037. https://doi.org/10.3390/nano11113037.
- Miranda, C.R., De Lara, L.S., Tonetto, B.C., 2012. Stability and mobility of functionalized silica nanoparticles for enhanced oil recovery applications. SPE International Oilfield Nanotechnology Conference, Huelva, Spain, pp. 311–321. https://doi.org/10.2118/157033-MS.
- Okon, A.N., Udoh, F.D., Bassey, P.G., 2014. Evaluation of rice husk as fluid loss control additive in water-based drilling mud. SPE Nigeria Annual International Conference and Exhibition, Lagos, Nigeria, pp. 391–400. https://doi.org/10.2118/172379-MS.
- Oseh, J.O., Mohd Norddin, M.N.A., Ismail, I., Gbadamosi, A.O., Agi, A., Mohammed, H.N., 2019. A novel approach to enhance rheological and filtration properties of water—based mud using polypropylene—silica nanocomposite. J. Pet. Sci. Eng. 181, 106264. https://doi.org/10.1016/j.petrol.2019.106264.
- Pang, S., Yang, X., Zhu, L., An, Y., 2025. Zwitterionic polymer grafted nano-SiO₂ as fluid loss agent for high-temperature water-based drilling fluids. J. Mol. Liq. 417, 126542. https://doi.org/10.1016/j.molliq.2024.126542.

- Petit, L., Bouteiller, L., Brûlet, A., Lafuma, F., Hourdet, D., 2007a. Responsive hybrid self-assemblies in aqueous media. Langmuir 23 (1), 147–158. https://doi.org/10.1021/la061466j.
- Petit, L., Karakasyan, C., Pantoustier, N., Hourdet, D., 2007b. Synthesis of graft polyacrylamide with responsive self-assembling properties in aqueous media. Polymer 48 (24), 7098–7112. https://doi.org/10.1016/j.polymer.2007.09.040.
- Portehault, D., Petit, L., Pantoustier, N., Ducouret, G., Lafuma, F., Hourdet, D., 2006. Hybrid thickeners in aqueous media. Colloids Surf., A 278 (1–3), 26–32. https://doi.org/10.1016/j.colsurfa.2005.11.089.
- Powell, J.W., Parks, C.F., Seheult, J.M., 1991. Xanthan and Welan: the effects of critical polymer concentration on rheology and fluid performance. SPE International Arctic 55 Technology Conference, Anchorage, Alaska. https://doi.org/10.2118/ 22066-MS.
- Raipuria, V., Rani, N., Sharma, V.P., Naiya, T.K., 2018. Use of nanoparticles derived from natural source and its application in drilling fluid. Int. J. Oil, Gas and Coal Technology 19 (3), 283–295. https://doi.org/10.1504/IIOGCT.2018.095572.
- Roustaei, A., Saffarzadeh, S., Mohammadi, M., 2013. An evaluation of modified silica nanoparticles' efficiency in enhancing oil recovery of light and intermediate oil reservoirs. Egyptian Journal of Petroleum 22 (3), 427–433. https://doi.org/ 10.1016/j.ejpe.2013.06.010.
- Sadeghalvaad, M., Sabbaghi, S., 2015. The effect of the TiO₂/polyacrylamide nanocomposite on water-based drilling fluid properties. Powder Technol. 272, 113–119. https://doi.org/10.1016/j.powtec.2014.11.032.
- Salami, O.T., Plank, J., 2016. Influence of electrolytes on the performance of a graft copolymer used as fluid loss additive in oil well cement. J. Pet. Sci. Eng. 143, 86–94. https://doi.org/10.1016/j.petrol.2016.02.021.
- Salih, A.H., Elshehabi, T.A., Bilgesu, H.I., 2016. Impact of nanomaterials on the rheological and filtration properties of water-based drilling fluids. SPE Eastern Regional Meeting. Canton, Ohio, USA. https://doi.org/10.2118/184067-MS.
- Sanchez, C., Julián, B., Belleville, P., Popall, M., 2005. Applications of hybrid organic-inorganic nanocomposites. J. Mater. Chem. 15 (35–36), 3559–3592. https://doi.org/10.1039/B509097K.
- Shaikh, S.M.R., Nasser, M.S., Magzoub, M., Benamor, A., Hussein, I.A., El-Naas, M.H., Qiblawe, H., 2018. Effect of electrolytes on electrokinetics and flocculation behavior of bentonite-polyacrylamide dispersions. Appl. Clay Sci. 158, 46–54. https://doi.org/10.1016/j.clay.2018.03.01.
- Shu, Y., Yan, J., 2008. Characterization and prevention of formation damage for fractured carbonate reservoir formations with low permeability. Pet. Sci. 5 (4), 326–333. https://doi.org/10.1007/s12182-008-0055-8.
- Smith, S.R., Rafati, R., Sharifi Haddad, A., Cooper, A., Hamidi, H., 2018. Application of aluminium oxide nanoparticles to enhance rheological and filtration properties of water-based muds at HPHT conditions. Colloids Surf., A 537, 361–371. https:// doi.org/10.1016/j.colsurfa.2017.10.050.
- Song, K., Wu, Q., Li, M., Ren, S., Dong, L., Zhang, X., Lei, T., Kojima, Y., 2016a. Water-based bentonite drilling fluids modified by novel biopolymer for minimizing fluid loss and formation damage. Colloids Surf., A 507, 58–66. https://doi.org/10.1016/j.colsurfa.2016.07.092.
- Song, K., Wu, Q., Li, M.C., Wojtanowicz, A.K., Dong, L., Zhang, X., Ren, S., Lei, T., 2016b. Performance of low solid bentonite drilling fluids modified by cellulose nanoparticles. J. Nat. Gas Sci. Eng. 34, 1403–1411. https://doi.org/10.1016/ j.jngse.2016.08.036.
- Stamatakis, E., Young, S., De Stefano, G., 2013. Meeting the ultrahigh-temperature/ ultrahigh-pressure fluid challenge. SPE Drill. Compl. 28 (1), 86–92. https:// doi.org/10.2118/153709-PA.
- Tchameni, A.P., Djouonkep, L.D.W., Nagre, R.D., Wang, X., 2024a. Thermo-responsive polymer-based Janus biogenic-nanosilica composite, part B: experimental study as a multi-functional synergistic shale stabilizer for water-based drilling fluids. J. Mol. Liq. 395, 123921. https://doi.org/10.1016/j.molliq.2023.123921.
- Tchameni, A.P., Nagre, D.R., Yin, S., Wang, L., Wang, X., Zhou, S., Hou, G., Wang, X., 2025. Thermo-responsive polymer-based Janus biogenic-nanosilica composite, part A: synthesis and colloidal behaviour in the presence of co-solutes. J. Mol. Liq. 421, 126909. https://doi.org/10.1016/j.molliq.2025.126909.
- Tchameni, A.P., Xie, B., Li, Y., Liu, W., Zhao, L., Luo, M., Wen, J., 2021a. Thermoassociating polymers based on cross-linked 2-acrylamido-methylpropane sulfonic acid, part B: effect of co-solutes on solution behavior. Colloids Surf., A 608, 125531. https://doi.org/10.1016/j.colsurfa.2020.125531.
- Tchameni, A.P., Xie, B., Ma, J., Wang, Y., Zhao, L., Xie, L., Luo, M., Wen, J., 2021b. Thermo-associating copolymer based on cross-linked 2-acrylamido-methyl-propane sulfonic acid, part C: experimental study into the performance of

- deepwater aqueous drilling fluids. Colloids Surf. 612, 125965. https://doi.org/10.1016/j.colsurfa.2020.125965.
- Tchameni, A.P., Xie, B., Zhang, H., Zhao, L., Luo, M., Wen, J., 2020. Thermo-associating polymers based on cross-linked 2-acrylamido-methylpropane sulfonic acid, part A: synthesis and solution behavior. Colloids Surf., A 593, 124611. https://doi.org/10.1016/j.colsurfa.2020.124611.
- Tchameni, A.P., Zhuo, L.Y., Wandji Djouonkep, L.D., Nagre, D.R., Chen, L.X., Zhao, L., Ma, C., Xie, B., 2024b. A novel responsive stabilizing Janus nanosilica as a nanoplugging agent in water-based drilling fluids for exploiting hostile shale environments. Pet. Sci. 21 (2), 1190–1210. https://doi.org/10.1016/j.petsci.2023.10.008.
- Tehrani, A., Gerrard, D., Young, S., Fernandez, J., 2009. Environmentally friendly water-based fluid for HPHT drilling. SPE International Symposium on Oilfield Chemistry, The Woodlands, Texas. https://doi.org/10.2118/121783-MS.
- Temraz, M.G., Hassanien, I., 2016. Mineralogy and rheological properties of some Egyptian bentonite for drilling fluids. J. Nat. Gas Sci. Eng. 31, 791–799. https://doi.org/10.1016/j.ingse.2016.03.072.
- Traciak, J., Zyła, G., 2022. Effect of nanoparticles saturation on the surface tension of nanofluids. J. Mol. Liq. 363, 119937. https://doi.org/10.1016/j.molliq.2022.119937.
- Umeda, J., Kondoh, K., 2010. High-purification of amorphous silica originated from rice husks by combination of polysaccharide hydrolysis and metallic impurities removal. Ind. Crops Prod. 32 (3), 539–544. https://doi.org/10.1016/ j.indcrop.2010.07.002.
- Vallejo, J.P., Żyła, G., Fernández-Seara, J., Lugo, L., 2019. Influence of six carbon-based nanomaterials on the rheological properties of nanofluids. Nanomaterials 9 (2), 1–19. https://doi.org/10.3390/nano9020146.
- Vandenberg, E.T., Bertilsson, L., Liedberg, B.O., Uvdal, K., Erlandsson, R., Elwing, H., 1991. Structure of 3-aminopropyl triethoxy silane on silicon oxide. J. Colloid Interface Sci. 1 (147), 103–118. https://doi.org/10.1016/0021-9797(91)90139-Y. Werner, B., Myrseth, V., Saasen, A., 2017. Viscoelastic properties of drilling fluids and
- Werner, B., Myrseth, V., Saasen, A., 2017. Viscoelastic properties of drilling fluids and their influence on cuttings transport. J. Pet. Sci. Eng. 156, 845–851. https:// doi.org/10.1016/j.petrol.2017.06.063.
- William, J.K.M., Ponmani, S., Samuel, R., Nagarajan, R., Sangwai, J.S., 2014. Effect of CuO and ZnO nanofluids in xanthan gum on thermal, electrical and highpressure rheology of water-based drilling fluids. J. Pet. Sci. Eng. 117, 15–27. https://doi.org/10.1016/j.petrol.2014.03.005.
- Wandji Djouonkep, L.D., Xie, B., Tao, H., Chen, J., Zhuo, L., Songwe Selabi, N.B., Zhao, L., 2024. Enhanced amphoteric polymer filtration reducer with vinyl-functionalized nanosilica for high-salt and ultra-high temperature water-based drilling environments. Geoenergy Science and Engineering 236, 212743. https://doi.org/10.1016/j.geoen.2024.212743.
- Xie, B., Chen, J., Chen, J., Ma, C., Zhao, L., Tchameni, A.P., 2023. Novel thermoassociating polymer/silica nanocomposite as a temperature-resistant rheology modifier for bentonite-free water-based drilling fluids. Geoenergy Science and Engineering 222, 211426. https://doi.org/10.1016/j.geoen.2023.211426.
- Xie, B., Liu, X., 2017. Thermo-thickening behavior of LCST-based copolymer viscosifier for water-based drilling fluids. J. Pet. Sci. Eng. 154, 244–251. https:// doi.org/10.1016/j.petrol.2017.04.037.
- Xie, B., Liu, X., Wang, H., Zheng, L., 2016. Synthesis and application of sodium 2-acrylamido-2-methylpropane sulphonate/N-vinylcaprolactam/divinyl benzene as a high-performance viscosifier in water-based drilling fluid. J. Appl. Polym. Sci. 133 (43), 1–12. https://doi.org/10.1002/app.44140.
- Zamani, H., Jafari, A., Mousavi, S.M., Darezereshki, E., 2020. Biosynthesis of silica nanoparticle using Saccharomyces cervisiae and its application on enhanced oil recovery. J. Pet. Sci. Eng. 190, 107002. https://doi.org/10.1016/ j.petrol.2020.107002.
- Zhang, Y., Qiu, Z., Mu, J., Ma, Y., Zhao, X., Zhong, H., Huang, W., Guo, P., 2021. Intelligent temperature-control of drilling fluid in natural gas hydrate formation by nano-silica/modified n-alkane microcapsules. Nanomaterials 11 (9), 2370. https://doi.org/10.3390/nano11092370.
- Zhao, J., Milanova, M., Warmoeskerken, M.M.C.G., Dutschk, V., 2012. Surface modification of TiO2 nanoparticles with silane coupling agents. Colloids Surf., A 413, 273–279. https://doi.org/10.1016/j.colsurfa.2011.11.033.
- Zhong, H., He, Y., Yang, E., Bi, Y., Yang, T., 2022. Modeling of microflow during viscoelastic polymer flooding in heterogenous reservoirs of Daqing Oilfield. J. Pet. Sci. Eng. 210, 110091. https://doi.org/10.1016/j.petrol.2021.110091.
- Zhu, D., Wei, L., Wang, B., Feng, Y., 2014. Aqueous hybrids of silica nanoparticles and hydrophobically associating hydrolyzed polyacrylamide used for EOR in high-temperature and high-salinity reservoirs. Energies 7 (6), 3858–3871. https://doi.org/10.3390/en7063858.